IJNT

International Journal of

Nanotechnology

INDERSCIENCE
PUBLISHERS
www.inderscience.com

Nanolasers: Lasing from nanoscale quantum wires

Samuel S. Mao

Advanced Laser Technologies Group, Lawrence Berkeley National Laboratory, University of California, CA 94720, Berkeley
E-mail: ssmao@lbl.gov

Abstract: Semiconductor lasers are in many ways second only to transistors as to their impact on today's high-tech industries. The unique characteristics, such as narrow emission wavelength, high frequency modulation, and device integratibility, make semiconductor lasers ideal photon sources for applications as diverse as telecommunication, signal processing, material characterization, and medical diagnostics. Advances in material growth technologies, particularly molecular beam epitaxy, metal-organic chemical vapor deposition, and a suite of chemical synthesis techniques, make the fabrication of high quality nanometer scale semiconductor structures possible. Thanks to the quantum size effects that drastically modify the energy spectra of confined electrons in reduced dimensions, the population inversion necessary for lasing action occurs more efficiently as the active semiconductor gain medium is scaled down from the bulk to the nanometer scale. Consequently, semiconductor lasers built with nanoscale active media are expected to exhibit extraordinary features such as great color range, high optical gain, and low lasing threshold. Indeed, miniaturized lasers using nanoscale semiconductor gain media – two-dimensional quantum wells, one-dimensional quantum wires, and zero-dimensional quantum dots – have shown significant improvements in device performance. This article provides an overview of the physics and technologies behind the rapid progress of miniaturization of semiconductor lasers, in particular the quantum wire lasers based on one-dimensional nanoscale optical gain media. Since the first report of lasing in quantum wires by Kapon and his co-workers [1], quantum wire lasers have evolved from 'microlasers' in which the one-dimensional nanostructure is embedded in a micron size optical cavity, to 'nanolasers' in which, as we recently demonstrated [2], the material gain and optical feedback are simultaneously achieved by individual nanoscale quantum wires. One-dimensional semiconductor fabrication technologies based on nanoscale lithography, self-organization, selective growth, and chemical synthesis will be reviewed along with recent advances of quantum wire lasers built upon each of these fabrication technologies.

Keywords: one-dimensional nanostructure; quantum wire; nanowire; semi-conductor laser; quantum confinement.

Reference to this paper should be made as follows: Mao, S.S. (2004) 'Nanolasers: Lasing from nanoscale quantum wires', *International Journal of Nanotechnology*, Vol. 1, Nos. 1/2, pp.42–85.

Biographical notes: Samuel S. Mao is a Scientist at the Lawrence Berkeley National Laboratory. He obtained his Ph.D. degree in Engineering from the University of California at Berkeley in 2000. His current research involves the development of nanoscale structures and devices, near field microscopy, and ultrafast laser technologies. In 2000, he performed the seminal optical experiment that demonstrated the first nanolaser – lasing from nanowires. He has contributed over 40 technical publications and delivered invited lectures at many conferences and universities.

1 Introduction

Miniaturization has often been a key word for modern integrated circuits built upon the concept that the smaller the device, the faster it operates. A similar line of thought is equally valid for semiconductor lasers that have been widely used in applications ranging from telecommunications to consumer electronics. Apparently, miniaturization will allow more lasers to be packed together and integrated with the shrinking integrated circuits.

The benefits of miniaturized semiconductor lasers are far beyond the capability of dense integration. In fact, size reduction results in improved device performance and new functionality. The basis of semiconductor laser operations [3–5] depends on the creation of nonequilibrium populations of energy carriers (electrons and holes, or excitons) in a semiconductor gain material, and coupling of electrons and holes to an optical field that stimulates radiative light emission. Quantum phenomena emerge when the dimension of a semiconductor material is scaled down to nanometer regime (< 100 nm); the resulting dramatic change of the physical properties of the nanoscale gain material has fueled global efforts to build high performance semiconductor 'nanolasers'.

1.1 Semiconductor laser cavities

Two basic elements necessary for realizing a semiconductor laser (Figure 1) include an *active gain medium* that provides optical gain by stimulated emission, and an *optical resonant cavity* that confines the photons to create positive optical feedback. Pumped by either an electrical or optical energy, electrons and holes within the semiconductor gain material can be excited to nonequilibrium energy levels so light radiation can be amplified (positive gain). If the resulting gain is sufficient to overcome the losses of the optical cavity that provides the necessary feedback of the radiation, lasing oscillation can be established at a well-established threshold. While the focus of this review is one-dimensional nanoscale structures – nanoscale quantum wires – as the active gain media of semiconductor lasers, it is beneficiary to take a brief look at different optical cavities that facilitate lasing action of nanoscale semiconductors.

Figure 1 Basic elements of a laser – gain medium and optical cavity

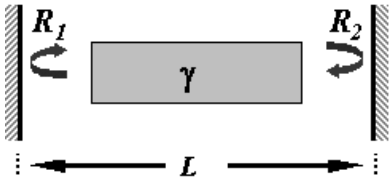

Conventional edge-emitting semiconductor lasers have an in-plane optical cavity with a cleaved facet mirror (Figure 2(a)). Light emission takes place from one side (edge) of the Fabry-Perot cavity typically a few hundred μm long (longitudinal) and 10 μm wide (lateral). Although the edge-emitting lasers have been used for many practical applications, the combination of edge emission and active layer geometry has several disadvantages. The long optical cavity results in typically multimode operation, by which the spontaneous emission of the active gain material is distributed over a large number of non-lasing modes. Because the active region is transversely thin (vs. laterally wide) for

carrier and photon confinement, edge-emitting lasers have highly elongated near and far fields. Additionally, edge-emitting semiconductor lasers are limited from being made smaller because they cannot be cleaved much shorter than 100 μm on a manufacturing basis.

Figure 2 Four basic types of semiconductor laser cavities

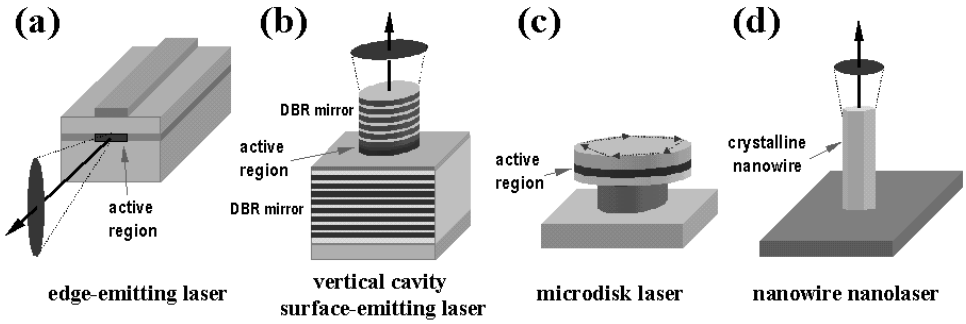

There have been several innovative designs of optical cavities aimed at overcoming the disadvantages of edge emission by confining photons in a smaller (microscale) volume. Once the optical cavity becomes sufficiently small, only one optical mode is within the emission bandwidth, as implied by the free spectral range ($\Delta\lambda$) of a laser cavity with length L,

$$\Delta\lambda = \frac{\lambda_0^2}{2nL}, \tag{1}$$

where λ_0 is the light wavelength, $\Delta\lambda$ represents the wavelength separation of the cavity mode, and n is the refractive index.

The vertical cavity surface emitting laser [6] (VCSEL), originally demonstrated in 1979 [7–9], was one of the first semiconductor laser cavities with dimensions on the order of the wavelength of light. As shown in Figure 2(b), VCSEL structures, including mirrors and active regions, are defined by layered structures, unlike edge-emitting laser cavities where mirrors are implemented by cleaved facets (or by etched gratings). The very short cavity length makes VCSEL operation inherently single longitudinal mode, in contrast to edge-emitting lasers with typical cavity length several hundred times of the lasing wavelength. The significant reduction in the gain length in VCSELs is compensated by a high quality factor cavity; the quality factor represents the ratio of the amount of energy stored in an optical cavity in the form of a standing wave to the amount of energy lost during a round trip inside the cavity. The development of distributed Bragg reflectors (DBR) with reflectivity close to 100% [10] allows the active region to contain as little as a single quantum well [11]. With laser emission from the wafer surface, it is possible to have a symmetric beam profile with very small divergence. Surface emission also favors the fabrication of two-dimensional laser arrays of coherent light sources. Additionally, the epitaxial growth techniques for the VCSEL mirrors make wafer-scale device testing possible, enabling high volume manufacturing. The development of

VCSELs has resulted in devices that have characteristics and reliability suitable for various commercial applications. Low threshold current and high operating efficiency have been achieved by constructing smaller active areas (e.g., ~μm^2) [12], band-gap engineering of the mirror stacks [13–15], and introducing confinement apertures to reduce optical losses [16].

The DBR mirrors of VCSEL cavities are essentially one-dimensional photonic crystals. Alternatively, two- and three-dimensional photonic crystals have been applied to provide effective control of light on the microscale [17–18]. In general, a photonic crystal consists of a dielectric medium that is patterned into a regular structure with a length scale on the order of the optical wavelength. For a proper crystal design, light is Bragg-scattered by the periodic structure and cannot propagate in any direction within the crystal. In analogy to the electronic band-gap in a semiconductor material, the range of optical frequencies that are excluded from the material is called the photonic band-gap. Like a semiconductor material, a defect in a photonic crystal will lead to a localized photon state within the band-gap, which can serve as an optical cavity with a small mode volume. Notably, photonic crystal defect laser cavities with various designs and sizes have been realized [19–23]. By introducing a single-defect photonic crystal, a wave-guide forms around the central defect region where the effective index is larger than the surrounding region.

Different from the photonic crystal type cavities, a microdisk laser [24] uses total internal reflection at the edge of a high refractive index disk (Figure 2(c)) to form low-loss whispering gallery type modes, in analogy to long distance travel of whispers (sound wave) along a curved inner surface. The laser operates by confining the light through total internal reflection, reflected repeatedly from the boundary with the same angle of incidence. As compared to Fabry-Perot laser cavities, microdisk cavities exhibit higher (10^4) quality factor, leading to enhancement of the spontaneous emission [25]. However, It is usually difficult to couple the light into useful directions since the light in microdisk structures tends leak out in all directions due to scattering of surface imperfections.

Perhaps the smallest Fabry-Perot type optical cavity that can effectively provide positive feedback of stimulated emission belongs to single crystalline nanowires having a length on the order of light wavelength (Figure 2(d)). Surface-emitting lasing action has been recently demonstrated in semiconductor nanowires [2] in which two crystalline facets serve as reflecting mirrors of the cavity. The realization of the nanowire nanolasers opens up a new and plausible route for achieving simultaneous carrier and photon confinement in one-dimensional nanoscale cavities. In general, the mode density in an optical cavity depends on the dimension of the cavity in a manner similar to that of the electron density of states due to quantum confinement. While the benefits of carrier confinement will be examined in the following sections, photon confinement in miniature optical cavities can lead to significant enhancement of the spontaneous emission rate [26]. Spontaneous emission is no longer an intrinsic material property, but rather is directly proportional to the density of electromagnetic modes with which a spontaneously emitted photon can couple. This cavity quantum electrodynamics phenomenon can provide a mechanism to realized low threshold semiconductor lasers as well as single photon sources [27].

1.2 Scope of the review

This article provides an overview of the advancement of semiconductor lasers based on nanoscale semiconductor materials. The focus here is semiconductor lasers with one-dimensional nanoscale structures – nanoscale quantum wires – as the active gain media. Quantum wires are anisotropic nanocrystals with diameter between 1 and 100 nm and length as long as a few microns. In these one-dimensional nanostructrues, carriers are localized in two directions, moving freely only along the wire axis. The additional carrier confinement in quantum wires over conventional two-dimensional quantum well structures is expected to result in semiconductor lasers with characteristics superior to quantum well lasers. The remaining of this review is organized as follows: Section 2 discusses the physics behind nanoscale semiconductor gain media; Section 3 provides an overview of different nanoscale quantum wire fabrication techniques that have led to the realization of lasing through optical or electrical pumping; Section 4 reviews various types of semiconductor quantum wire lasers; and Section 5 is a perspective of semiconductor lasers based on nanoscale semiconductor structures.

2 Lasing from nanostructures – the motivations

The primary motivations behind developing miniaturized semiconductor lasers are substantial performance improvements [28–31] as the size is scaled down to the nanometer regime. This section intends to provide a basic understanding of the emerging physical phenomena associated with quantum confinement in active semiconductor gain media with reduced dimensions. The physics behind improved lasing characteristics – greater color range, higher material gain, and lower lasing threshold – in semiconductor lasers based on nanoscale gain media will be illustrated. In the discussion of the benefits of a reduced lasing threshold, direct current injection will be assumed as the pumping mechanism.

2.1 Greater color range

One attractive feature of nanoscale materials stems from the fact that electrons and holes are confined in a small region to produce discrete energy levels. The use of nanoscale materials with size-dependent discrete transition energy levels provides a means of tuning the wavelength of semiconductor light emission. In principle, any color emission, from the far-IR to the near-UV, is possible by changing materials as well as their size. Semiconductor lasers with widely tunable wavelength ranges are essential for applications like high-capacity wavelength division multiplexed (WDM) fiber communication systems [32].

2.1.1 Spherical nanocrystals – an example

One classical example of changes in the light emission wavelengths resulting from small variations in the size of the nanostructure is the color of nanoscale CdSe [33], one of the most developed nanocrystals. CdSe exhibits red color for a ‘large’ (e.g., 3 nm) nanocrystal but turns yellow at approximately half the size. Quantum confinement generally shifts the optical transitions to higher energies (blue shift, shorter wavelength). Figure 3 shows the lasing spectra of semiconductor lasers using CdSe nanocrystals of different radius as the active gain media [31].

Figure 3 Lasing spectra (80 K) of nanocrystal lasers with different crystal radius: 2.7 nm (a), 2.4 nm (b), 2.1 nm (c), and 1.7 nm (d). The active lasing media are CdSe nanocrystals except for (d), CdSe/ZnS core/shell nanocrystals. (After reference [31])

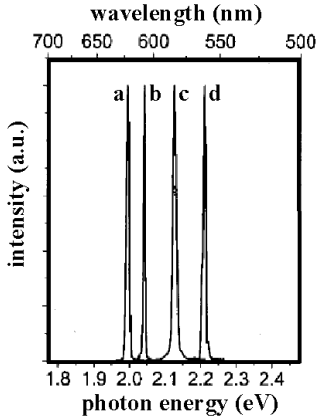

Light emission characteristics of semiconductor materials are strongly influenced by the transitions between electron and hole energy levels; a simple quantum mechanical model of electrons and holes can be used to illustrate the size-dependent behavior of nanoscale semiconductor materials. The motion of electrons is controlled in nanoscale structures by enforcing a restriction on them in terms of potential barriers, which prevent electrons and holes from moving in certain directions. For a spherical nanocrystal surrounded by an infinite potential barrier, by solving the three-dimensional Schrödinger equation, the electron and hole energy levels, characterized by an angular momentum quantum number l, can be written as [34],

$$E_{n,l} = \frac{\hbar^2 \phi_{n,l}^2}{2ma^2}, \tag{2}$$

with $n = 1, 2, 3 \ldots$ and $l = 0, 1, 2 \ldots$. In the above expression, $\hbar$ is the Planck's constant, m represents the electron or hole effective mass, a is the nanocrystal radius, $\phi_{n,l}$ is the nth root of the spherical Bessel function of order l, $j_l(\phi_{n,l}) = 0$, with $\phi_{1,0} = \pi$. The energy levels of the nanocrystals are discrete, as dictated by the quantum number n and l. The energies of the lowest electron and hole levels scale with the square of the inverse radius of the nanocrystal (a). An increase of nanocrystal band-gap energy with respect to the bulk material band-gap can be obtained as,

$$E_g^{\text{nanocrystal}} = E_g^{\text{bulk}} + \frac{\hbar^2 \pi^2}{2m_r a^2}, \tag{3}$$

where $m_r = m_e m_h/(m_e + m_h)$ is the reduced effective mass of the electron-hole pair. As a consequence, the photon energy of the band edge optical transition increases, which gives rise to a dramatic color change in nanocrystals. For CdSe nanocrystals, the energy gap can shift from 1.8 eV (bulk value) to approximately 3.0 eV, covering almost the whole visual part of the optical spectrum.

Strictly speaking, one needs to include coulomb interactions between the electron and the hole inside a nanoscale material and adopt the concept of exciton – the electrically bonded electron-hole pair. In doing so, the lowest excitation energy needs to be modified [35–36] as

$$\left\{\frac{\hbar^2\pi^2}{2m_r a^2}\right\}_{\text{free}} \rightarrow \left\{\frac{\hbar^2\pi^2}{2m_r a^2} - \frac{1.8e^2}{\varepsilon a}\right\}_{\text{bond}}, \tag{4}$$

where e is the electric charge and ε is the dielectric constant of the semiconductor. In the rest of this section, we will primarily apply the free electron and hole model to illustrate basic physics concepts underlying the improvement of semiconductor laser performance resulting from reduced dimensions.

2.1.2 Quantum confinement in one, two, and three dimensions

Other than spherical potential barriers, one-, two-, and three-dimensional quantum confinement can be achieved in 'film', 'wire', and 'box' like geometries, characterized by length scales L_x, L_y, and L_z in three separate directions. It has been customary in literature to name these nanostructures 'quantum wells', 'quantum wires', and 'quantum dots', respectively. In the case of infinitely deep rectangular potential barriers in each restricted dimension, the energies of the confined carriers with respect to the band edges can be written in the form [37],

$$E_l = \frac{\pi^2\hbar^2 l}{2mL_x^2} + \frac{\hbar^2(k_y^2 + k_z^2)}{2m}, \text{ (quantum wells)} \tag{5a}$$

$$E_{l,m} = \frac{\pi^2\hbar^2}{2m}\left(\frac{l^2}{L_x^2} + \frac{m^2}{L_y^2}\right) + \frac{\hbar^2 k_z^2}{2m}, \text{ (quantum wires)} \tag{5b}$$

$$E_{l,m,n} = \frac{\pi^2\hbar^2}{2m}\left(\frac{l^2}{L_x^2} + \frac{m^2}{L_y^2} + \frac{n^2}{L_z^2}\right), \text{ (quantum dots)} \tag{5c}$$

where $l, m, n = 1, 2, 3 \ldots$ are quantum numbers of the energy levels due to carrier confinement in x, y, and z directions, respectively, $k_{x,y,z}$ are the wave vectors, and $\hbar^2 k_{x,y,z}^2 / 2m$ represent kinetic energies in the direction of unconfined dimensions. A bulk semiconductor can be regarded as an object in which carriers move freely in all three dimensions; the kinetic energy is thus given by

$$E = \frac{\hbar^2(k_x^2 + k_y^2 + k_z^2)}{2m}. \text{ (bulk)} \tag{5d}$$

As seen from the above equations, subbands exist in quantum wells or quantum wires in addition to the quantization energies, because the carriers are free to move in two or one dimensions. In a quantum dots, the carriers have no freedom of movement and only discrete (atomic like) states are formed.

2.2 Higher material gain

Gain enhancement in semiconductor materials due to quantum confinement in one, two, and three directions has been investigated theoretically since 1982 [28]. Resulting from the narrowing of the carrier density of states, the laser gain profile of nanoscale semiconductor media was predicted to be concentrated into a much narrower spectral region than the corresponding bulk materials.

2.2.1 Density of states

One principal advantage of nanoscale semiconductor materials for laser applications originates from a noticeable increase of the density of states $\rho(E)$ for electrons and holes with the reduction of dimensions (Figure 4). The density of states is a material property which quantifies the number of carriers that are permitted to occupy a given energy state of the semiconductor. Since most semiconductor lasers operate near the conduction band minimum, the density of states of a semiconductor material imposes an intrinsic limitation on the number of carriers that are allowed to contribute to the lasing performance at one time. The expressions of the density of states per unit volume for electrons or holes in nanostructures of different dimensions as well in bulk (3D) have the form [37],

$$\rho_{2D}(E) = \frac{m}{\pi\hbar^2 L_x}\sum_l \Theta(E - E_l)\ , \text{(2D)} \tag{6a}$$

$$\rho_{1D}(E) = \frac{(2m)^{\frac{1}{2}}}{\pi\hbar L_x L_y}\sum_{l,m} (E - E_{l,m})^{-\frac{1}{2}}, \text{(1D)} \tag{6b}$$

$$\rho_{0D}(E) = \frac{2}{L_x L_y L_z}\sum_{l,m,n} \delta(E - E_{l,m,n})\ , \text{(0D)} \tag{6c}$$

and

$$\rho_{3D}(E) = \frac{(2m/\hbar^2)^{\frac{3}{2}}}{2\pi^2}\sqrt{E}\ , \text{(3D)} \tag{6d}$$

where Θ is the step function and δ is the delta-function.

For two-dimensional quantum wells, the carriers are free to move in the plane of the film, which gives the total density of states a characteristic staircase shape, replacing the parabolic shape of the bulk density of states. In the one-dimensional quantum wire case, the carriers are confined also in a second direction and they are free to move only along the wire axis. As a consequence of one-dimensional movement, the density of states has $1/E$ dependence for each of the discrete pairs of states in the confined directions. Lastly,

if the movement of the carriers is limited in all three directions, one has a zero-dimensional quantum dot for which the states are quantized in all directions and the density of states is a series of discrete, sharp states resembling that of an atom.

Figure 4 Schematic illustrations of the density of states for bulk (3D), quantum well (2D), quantum wire (1D), and quantum dot (0D) nanostructures. The contour characterized by a dashed curve in each case represents the occupied states at similar carrier densities

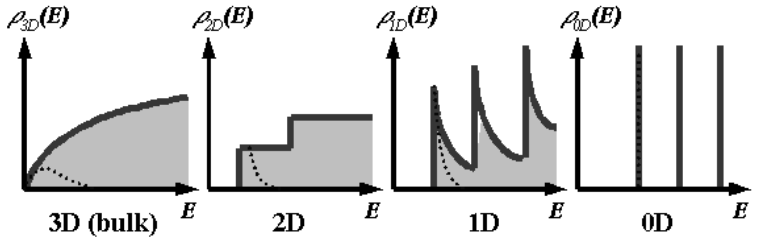

2.2.2 Material gain

Considering the three possible routes of radiative band-to-band transitions occurred in a semiconductor, from E_2 in the conduction band to E_1 in the valence band as shown schematically in Figure 5, the first process is spontaneous emission where a recombination of an electron-hole pair leads to the emission of a photon, random in direction, phase, and time. The second process is (stimulated) absorption; an electron-hole pair is generated as the result of the absorption of an incoming photon. The third process is stimulated emission; a recombination of an electron-hole pair is stimulated by a photon, with a second photon generated simultaneously, which has the same direction and phase as the first photon.

A net generation of coherent photons (positive gain) occurs if the rate of stimulated emission exceeds the rate of absorption. The optical gain of the material – the material gain, γ, can be defined as the proportional growth of the photon density (fractional increase of light intensity I_ω per unit length) as the light propagates along certain direction (e.g., z-direction) inside the medium (Figure 6),

Figure 5 Schematic illustrations of three possible routes of radiative band-to-band transition in a semiconductor material

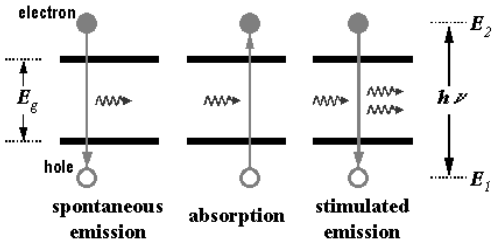

Figure 6 Optical gain (light amplification) in an active semiconductor medium

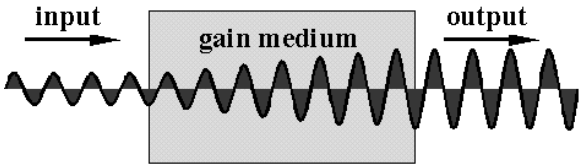

$$\gamma(\omega) = \frac{1}{I_\omega}\frac{\mathrm{d}I_\omega}{\mathrm{d}z}\,. \tag{7}$$

For semiconductors with effective population inversion due to electrons and holes, the gain function for optical transition from E_2 in the conduction band to E_1 in the valence band can be written as [5],

$$\gamma(\omega) = A_{21}\frac{\lambda^2}{8\pi n^2}\rho_{\mathrm{jnt}}(\hbar\omega)\left[f_C(E_2) - f_V(E_1)\right], \tag{8}$$

where $\hbar\omega$ is the photon energy, λ is the wavelength, n is the refractive index, A_{21} is the spontaneous emission coefficient, f_C and f_V are the quasi-Fermi functions for the conduction and valance bands, and $\rho_{\mathrm{jnt}}(\hbar\omega)$ is the joint density of states (defined using a reduce mass for electron-hole pairs) evaluated at $E = \hbar\omega$. The expression of the material gain in semiconductors suggests that an incoming light wave of photon energy $\hbar\omega$ is amplified (positive γ) if the condition $f_C(E_2) > f_V(E_1)$, or equivalently [38],

$$E_{FC} - E_{FV} > \hbar\omega > E_g\,, \tag{9}$$

is satisfied. The gain material becomes transparent ($\gamma = 0$) when the separation in the quasi-Fermi levels (E_{FC} and E_{FV}) equals the energy gap (E_g) between the highest and lowest available states for the electrons and holes. The carrier density required to provide this separation is known as the transparency carrier density, N_{tr}. Optical gain of the material is maintained when pumping the semiconductor creates a carrier density (N) larger than N_{tr}. The material gain can be approximated (near transparency) as

$$\gamma = \frac{\partial\gamma}{\partial N}\left(N - N_{\mathrm{tr}}\right) = \gamma'\left(N - N_{\mathrm{tr}}\right), \tag{10}$$

where γ' is the differential gain defined as the rate of gain increase as carriers are injected into the active medium. Notice that N_{tr} is not too different for nanostructures because it is determined by the relative locations of the quasi-Fermi levels at transparency, which are typically not too different between bulk and nanostructures.

The expression of the material gain (Equation (8)) indicates that γ is proportional to the products of the joint density of states of the semiconductor and the difference in the quasi-Fermi functions of the conduction and the valence band. The density of states has a more peaked structure with the decrease of the dimensionality, particularly for zero- and one-dimensional nanostructures (Figure 4). The major effect of the narrowing of the

density of states with reducing dimensionality is to confine the carrier energy distribution to narrower spectral regions (Figure 4). As a consequence, increasing quantum confinement yields narrowing of the gain spectrum (Figure 7), thus higher optical gain at a given carrier density. The differential gain γ' increases correspondingly, due to the narrowing of the gain spectrum.

Figure 7 Calculated room temperature gain spectra for GaInAs/InP quantum dot (QD), quantum wire (QWR), quantum well (QW), and bulk semiconductor active media. (After reference [29])

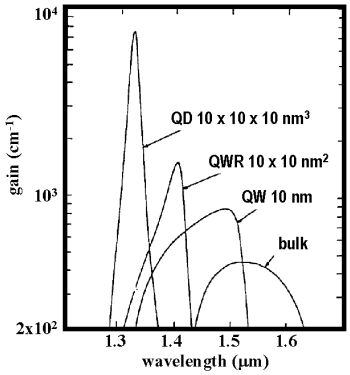

2.3 Lower lasing threshold

Threshold current density J_{th} is an important characteristic of a semiconductor laser device, at which gain overcomes overall (internal and external) losses thus enabling lasing. Lasing threshold can be reduced by making the active volume smaller and by modifying the density of states for the carriers, for example, through the use of a quantum well in the active region containing a single layer of quantum dots [39–41].

2.3.1 Threshold condition

To derive the threshold condition of semiconductor lasers, one needs to consider the total photon losses inside the optical cavity in addition to the optical gain of the active medium. A basic semiconductor laser structure consists of an active gain medium enclosed inside an optical cavity bounded by two reflecting mirror planes (Figure 1). The minimum material gain, γ_{th}, at which the device starts lasing operation can be estimated from the unity round trip condition when the gain provided to the optical mode compensates the intrinsic absorption and the mirror losses for a roundtrip,

$$R_1 R_2 \exp\left\{2(\Gamma\gamma_{th} - \alpha_i)L\right\} = 1, \tag{11}$$

where R_1 and R_2 are the mirror reflectivity, L is the laser cavity length, α_i is the internal loss, and Γ is the confinement factor characterizing the overlap of the lasing mode with the active region cross-section. Since only a part of the intensity profile of the optical mode overlaps with the semiconductor active region, one has to distinguish between the

gain of the active material γ and the gain (lower) of the optical mode $\Gamma\gamma$ reflecting light propagation in the entire device. Solving Equation (11) for the threshold gain γ_{th},

$$\Gamma\gamma_{\text{th}} = \alpha_i + \frac{1}{L}\ln\left(1/\sqrt{R_1 R_2}\right). \tag{12}$$

At the lasing threshold, the optical gain shall compensate the sum of the intrinsic absorption and the mirror losses, which depend on the cavity length and the mirror reflectivity. Combining Equation (12) and Equation (10), the threshold carrier density N_{th} can be written as,

$$N_{\text{th}} = N_{\text{tr}} + \frac{1}{\Gamma\gamma'}\left[\alpha_i + \frac{1}{L}\ln\left(1/\sqrt{R_1 R_2}\right)\right]. \tag{13}$$

The carrier density at the threshold needs to be high enough to achieve material transparency (N_{tr}) and overcome cavity losses simultaneously.

2.3.2 Threshold current density

For carrier injection type semiconductor lasers, since the rate at which the carriers are injected into the active region must equal the electron-hole recombination rate under steady state conditions, the injection current density J is related to the injected carrier density [42], N, as

$$J = \frac{eNL_z}{\eta\tau_R}, \tag{14}$$

where L_z is the active region thickness, τ_R is the carrier recombination time including contributions from radiative and nonradiative recombination, and η is the quantum efficiency characterizing the fraction of the injected carriers arriving in the active region. Using Equation (13) for the expression of N_{th}, the threshold current density can be written as

$$J_{\text{th}} = \frac{eL_z}{\eta\tau_R}\left\{N_{\text{tr}} + \frac{1}{\Gamma\gamma'}\left[\alpha_i + \frac{1}{L}\ln\left(1/\sqrt{R_1 R_2}\right)\right]\right\}, \tag{15}$$

i.e.,

$$J_{\text{th}} = J_{\text{th}}^{\text{mat}} + J_{\text{th}}^{\text{cav}} = \left\{\frac{eN_{\text{tr}}L_z}{\eta\tau_R}\right\}_{\text{mat}} + \left\{\frac{eL_z}{\eta\tau_R\Gamma\gamma'}\left[\alpha_i + \frac{1}{L}\ln\left(1/\sqrt{R_1 R_2}\right)\right]\right\}_{\text{cav}}. \tag{16}$$

The current necessary for lasing consists of two parts – $J_{\text{th}}^{\text{mat}}$, the current needed to maintain the carrier density at transparency in the semiconductor gain medium, and $J_{\text{th}}^{\text{cav}}$, the current needed to attain necessary gain to overcome losses inside the laser cavity. $J_{\text{th}}^{\text{mat}}$ represents a fundamental limit to achieving the lowest lasing threshold for semiconductor lasers, which is obtained with vanishing cavity losses.

In fact, part of the reduction of threshold current has its origin from a simple geometrical scaling of the physical size of the active region without invoking quantum confinement. As seen from Equation (14), since the threshold carrier density does not change significantly between bulk and nanostructures, it is essential to reduce the thickness of the active region L_z in order to decrease the threshold current density.

The advantage of using nanoscale quantum structures for reducing threshold current density lies not only in their small active volume, but also in larger differential gain γ' resulted from the confinement of the carrier energy distribution [43–45], as seen from the expression for $J_{\text{th}}^{\text{cav}}$. Further reduction of the threshold current density can be achieved by using tight optical confinement (large Γ) as well as reducing cavity losses. It is informative to plot the evolution trend [46] of the minimum threshold current densities achieved since the invention of semiconductor laser in early 1960s, as illustrated in Figure 8.

The reduction of the threshold current density, or threshold current ($I_{\text{th}} \propto J_{\text{th}}$), can yield many improvements in the performance of semiconductor lasers. A need in a variety of laser applications is high power conversion efficiencies, for instance. Because their threshold current can be very small, semiconductor lasers based on nanoscale semiconductor gain media are expected to have large above-threshold power conversion efficiency, η_p, which reflects the efficiency of a semiconductor laser in converting electrical power input to optical power,

$$\eta_p = \frac{P_0}{V_b I} = \eta_d \frac{E_g}{V_b}\left(1 - \frac{I_{\text{th}}}{I}\right), \tag{17}$$

where V_b is the input bias voltage, η_d is the differential quantum efficiency. Neglecting the spontaneous component of optical emission, $P_0 = \eta_d E_g (I - I_{\text{th}})$, denoting the above threshold optical power output. Additionally, due to a reduced threshold current, the modulation bandwidth of semiconductor lasers with nanoscale gain media could be very large. The modulation bandwidth of a semiconductor laser can be written as [42]

Figure 8 The trend of the reduction of semiconductor laser threshold

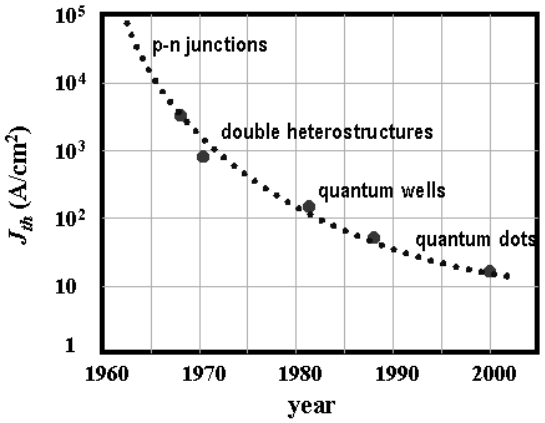

$$f_{3dB} = 1.55 f_r = \frac{1.55}{2\pi\tau_R}\sqrt{\frac{\tau_R}{\tau_p}\left(\frac{I}{I_{\text{th}}} - 1\right)}, \tag{18}$$

where f_r denotes the relaxation frequency and τ_p is the photon lifetime. Clearly, high-speed modulation, essential for communication applications of semiconductor lasers that are transmitting the vast flux of information over optical fibers, is possible with small I_{th} resulting from quantum confinement in nanoscale semiconductors.

The use of semiconductor quantum wells as the optical gain media represents the first generation semiconductor laser technology implementing nanoscale materials. A quantum well is a thin semiconductor layer (a few nanometers thick in the *z*-direction) sandwiched between layers of larger band-gap barriers. The band-gap difference causes electrons and holes to be trapped in the quantum well; the resulting confinement in the *z*-direction leads to discrete energy levels greater than that of a bulk material layer. Quantum confinement in quantum wells results in a step-like density of electronic states that is non-zero at the band edge, enabling a higher concentration of carriers to contribute to the band-edge emission and leading to a reduced lasing threshold and improved characteristics. A further enhancement in the density of states at the band edge and the associated reduction in the lasing threshold can be achieved with quantum wires and quantum dots where quantum confinement occurs in two and three separate directions, respectively. Semiconductor lasers with quantum wells [4] are relatively mature and many of their characteristics have been realized in commercial applications. In contrast, quantum wire and quantum dot structures are still in their development stage. One critical aspect for semiconductor lasers based on quantum dots is the statistical nature of the size and location, which gives rise to the broadening in the emission spectra. Progress of quantum dot lasers has been discussed in several recent reviews [46–49]. The focus of this article is semiconductor lasers based on one-dimensional nanoscale quantum wires.

3 Fabrication of one-dimensional nanostructures

Nanoscale semiconductor structures in which carriers are confined in more than one direction (quantum wires or nanowires) have unique properties suitable for high performance semiconductor laser applications. However, progress in the realization of practical quantum wire (and quantum dot) lasers has lagged behind advances in quantum well laser technology because the fabrication of nanoscale quantum wires with good crystalline characteristics has been a challenging task. Although a universal nanoscale quantum wire fabrication scheme for semiconductor laser applications is not available, optically or electrically pumped lasing has been achieved in nanoscale quantum wires produced by a variety of techniques developed over the past 15 years or so.

3.1 Development of nanoscale fabrication technologies

Semiconductor lasers based on two-dimensional quantum well structures represent the first generation nanoscale semiconductor laser technology. Their success is largely due to the breakthrough in two fabrication techniques, molecular-beam epitaxy (MBE) and metal-organic chemical vapor deposition (MOCVD), which allow for the deposition of semiconductor materials with atomic-layer precision. With nearly monolayer control

available in MBE and MOCVD, layers of different materials can be reproducibly grown with dimensions small enough to display quantum effects. These quantum well fabrication techniques have triggered a wide spectrum of experimental and theoretical investigations resulting in not only the observation of a number of intriguing new phenomena due to electronic quantization, but also the emergence of a new class of semiconductor laser devices.

MBE was developed in the early 1970s as a means of growing high-purity epitaxial layers of compound semiconductors [50–51]. In MBE, the constituent elements of a semiconductor in the form of 'molecular beams' are impinged, in ultra-high vacuum environment, onto a heated crystalline substrate to form thin epitaxial layers. The molecular beams are typically from thermally evaporated elements heated in effusion cells. Atomic layer-by-layer deposition, with typical growth rates of a few Å/s, is achieved by using low beam flux, controlled by varying the source temperature. The atomic mean-free path in the beams is usually larger than the distance between the source and the substrate; shutters in front of the individual sources are typically used to control growth time as well as the sequence of which material to grow. MBE can produce high-quality layers with precise control of quantum well thickness, doping, and composition.

MOCVD is one variation of chemical vapor deposition techniques that creates thin film material through the use of chemical reactions [52–53]. MOCVD is a gas phase technique usually operated at low pressure. Modified MOCVD technique [54] using the gas sources of MOCVD in a high vacuum molecular beam system also exists, which is also known as chemical beam epitaxy. A combination of organometallic compounds and hydrides (e.g., trimethylgallium and arsine for GaAs and trimethylgallium and ammonia for GaN) is typically used as the sources of elements for quantum wells. A typical MOCVD deposition process takes place through a series of basic steps that include transport of the reactants to the substrate surface, surface chemical reaction, surface migration and lattice incorporation, and transport of reaction products outside the deposition zone. The advantage of the MOCVD technique is relatively simple reactor design that enables the growth of quantum well heterostructures with abrupt hetero-boundaries and steep doping profiles by rapidly changing the vapor phase composition.

There are many different materials that can be grown by MBE and MOCVD to form quantum well structures. AlAs and GaAs have almost identical lattice constants, i.e., arbitrary structures can be grown with high quality in this materials system. Another commonly used system is InGaAs with InP; the proportions of In and Ga can be adjusted to yield a lattice constant for the ternary (three-component) InGaAs alloy that is equal to InP. Use of four component (quaternary) alloys (e.g., InGaAsP) offers sufficient degrees of freedom to adjust both the lattice constant and the band-gap energy of the material. Up to a certain critical thickness, which depends on the degree of lattice constant mismatch, it is possible to grow structures with materials that naturally have different lattice constants. Any material can accommodate a certain amount of elastic strain without generating dislocations or defects. The strained-layer structure will be thermodynamically stable if its thickness is small enough to maintain the elastic strain energy below the energy of dislocation formation. Strained-layer structures can display new electronic and optical properties and represent a tool for band structure modification in a predictable fashion [55].

Compared to the fabrication of quantum well structures, the realization of nanoscale quantum wires requires precise growth control in the lateral dimension. The following

sections review recent advances in one-dimensional fabrication technologies that have resulted in a variety of quantum wire laser structures. These nanoscale quantum wire fabrication techniques can be categorized as (1) nanoscale lithography, (2) self-organization, (3) selective growth, and (4) chemical synthesis.

3.2 Nanoscale lithography

Taking the advantage of well-developed quantum well fabrication technologies (MBE and MOCVD), the most straightforward method to realize one-dimensional nanostructures is etching (and re-growth) through wire-defining masks placed above the quantum wells [56–62]. This nanoscale lithography scheme offers significant flexibility in the design of arrays of quantum wires that can be incorporated in semiconductor laser cavities. However, despite the fact that etching has been a standard process for realization nanoscale transistor circuits, for optical applications, etching-induced lateral damage can degrade the light emission efficiency. These damages are nonradiative recombination centers that can dramatically reduce the optical gain of the quantum wires therefore suppress the lasing action. Clearly, the primary challenge involved in optimizing nanoscale lithography of quantum wire fabrication is the elimination of damages introduced during the etching and re-growth steps.

Significant improvements of quantum wire structures have been demonstrated recently by careful control of etching and re-growth steps [63–65]. Figure 9 is a schematic illustration of quantum wire fabrication process involving two-step deposition (e.g., MOCVD) [64]. Fabrication starts by first depositing a single or multiple-quantum wells on the top of the substrate. One-dimensional wire pattern is then formed by etching the quantum well active region through an electron-beam written mask layer (Figure 9(a)). After removing the mask layer, embedded growth of one-dimensional quantum wire heterostructures is performed by the second deposition process (Figure 9(b)). In forming the wire pattern, wet chemical etching can yield the least damages [66], however, the fabrication of quantum wires is usually limited to only one or two active layers because of their crystal orientation dependence. Dry etching such as the reactive ion-beam etching can be used to fabricate multiple layers of quantum wires, which are advantageous for low threshold laser operation, followed by wet chemical etching to remove damages induced by the high kinetic energy beams of the dry etching step.

Alternative to etching through wire-defining masks, implantation and diffusion under masks have also been applied to realize one-dimensional nanostructures based on pre-deposited quantum wells [67–68]. In these cases, the mask acts to prevent certain ion species from penetrating underneath, therefore generating a composition modulation in the form of nanoscale wires.

Figure 9 Quantum wire fabrication based on nanoscale etching and re-growth

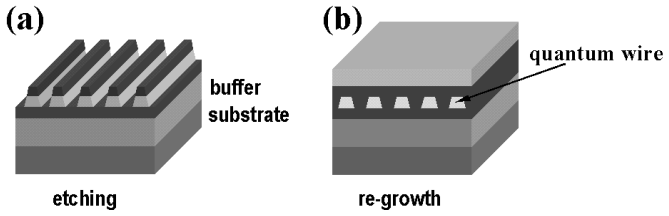

3.3 Self-organization

Different from nanoscale lithography that involves post-growth wire patterning, *in situ* self-organized growth of one-dimensional nanostructures has been developed. Self-organized growth methods are promising for semiconductor laser applications since high-density nanometer size quantum wires can be fabricated without introducing damages caused by etching. In addition, the size of self-organized quantum wires can be controlled simply by adjusting the growth and deposition conditions. Two primary self-organized quantum wire fabrication methods are strain-induced lateral ordering and epitaxial growth on vicinal surfaces.

3.3.1 Strain-induced lateral ordering (SILO)

One-dimensional quantum wire heterostructures can be self-organized by utilizing strain-induced lateral ordering process developed by Hsieh and co-workers in 1990 [69–70]. Quantum wire formation by strain-induced lateral ordering is based on lateral composition modulation, i.e., the spontaneous formation of phase-separated, self-organized periodic structures during the epitaxial growth of certain type of semiconductor thin films (e.g., short period superlattices). The origin of lateral composition modulation is still under debate, but it is generally agreed that it is a kinetic process involving surface diffusion and strain mechanisms. Using strain-induced lateral ordering that leads to periodic low band-gap and high band-gap regions, arrays of quantum wires have been fabricated in a variety of semiconductor compounds (e.g., InGaP, InGaAs, and AlInAs) with either MBE or MOCVD [71–75].

Figure 10 is a schematic diagram showing one-dimensional quantum wire formation through lateral modulation in InGaAs alloys deposited on an InP substrate [76]. A buffer layer of lattice-matched InGaAs is first grown on the substrate (Figure 10(a)), followed by the growth of a short period superlattice (Figure 10(b)) of $(InAs)_n/(GaAs)_m$ ($n, m \sim 2$), which is then capped with lattice matched InGaAs. The resulting structure is vertical sheets of alternately Ga-rich and In-rich nanoscale wire structure, laterally modulated in the [110] direction, exhibiting two-dimensional quantum confinement.

Figure 10 Formation of one-dimensional nanoscale quantum wires by strain-induced lateral ordering

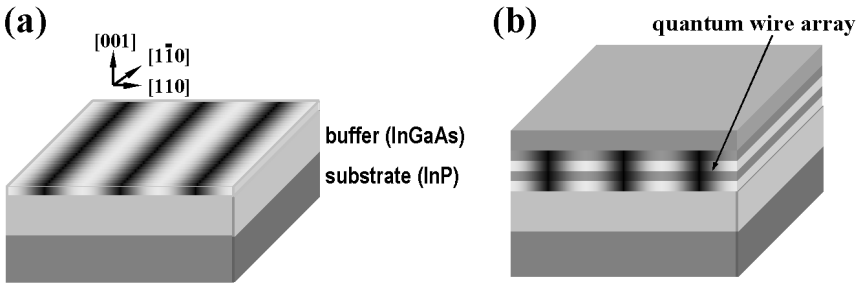

Figure 11 Growth of quantum wires on a vicinal surface with multiatomic steps

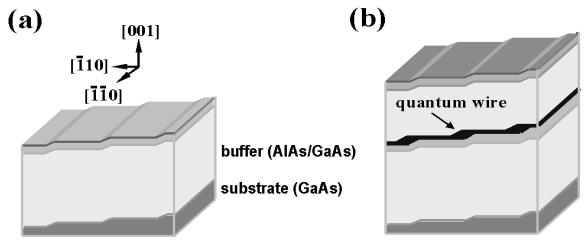

3.3.2 Epitaxial growth on vicinal surfaces

Epitaxial growth on vicinal substrates, as originally proposed by Petroff and co-workers [77], is another self-organization approach to create narrow quantum wire arrays without the use of lithography [78–83]. Quantum wires grown on vicinal surfaces are due to the existence of coherently aligned stepped surfaces and subsequent thickness modulation of the deposition layers at the multiatomic step edges. Figure 11 shows a schematic quantum wire array heterostructure fabricated using vicinal growth technique. A typical vicinal growth process for GaAs quantum wires starts by growing a buffer layers (e.g., AlAs/GaAs superlattice) on a slightly rnisaligned GaAs substrate (Figure 11(a)). Under proper deposition conditions, arrays of multiatomic steps form during superlattice growth on a misaligned substrate. The next step is depositing a single quantum well (e.g., AlAs/GaAs/AlGaAs) [80] or a fractional superlattice layer (e.g., $(AlAs)_{1/4}(GaAs)_{3/4}$) [83] to form a one-dimensional wire array (Figure 11(b)). A substrate misalignment of 2° can yield lateral periodicity of approximately 8 nm. Since the thickness of the GaAs layer at the step edges is usually thicker than that at the terraces, GaAs quantum wires are naturally formed at these step edges. Deposition interruption during the growth of GaAs layer may help GaAs migrate to the step edges [84].

Although the vicinal growth technique is attractive to yield dense quantum wire structures of high interface quality, its applications are limited due the strict requirement of preparing vicinal surfaces of multiatomic (or monatomic) steps with extremely high accuracy. Recent reports [81] of GaAs and InGaAs quantum wires grown on naturally corrugated high index planes of GaAs substrates appear promising. For example, the surface of GaAs (or InGaAs) grown on a (775)B GaAs substrate above a substrate temperature of 640°C (or 620°C) was found to be corrugated; subsequent growth of self-organized vicinal quantum wires has been achieved. Room temperature lasing has been reported [82] in semiconductor lasers using quantum wires active media grown on high index substrate planes.

3.4 Selective growth on pre-patterned substrates

As in the case of quantum wire growth on vicinal surfaces, flat or non-flat patterns generated using lithography can provide templates for direct growth of one-dimensional nanoscale structures. Epitaxial growth on pre-pattered substrates provides more flexibility than growth on vicinal surfaces in the design of quantum wires. Selectively grown quantum wires have been frequently fabricated on pre-patterned V-shape grooves and Λ-shape ridges, as well as T-shape cleaved edges of pre-deposited quantum well structures.

Figure 12 Selective growth of quantum wires on a pre-patterned V-groove substrate

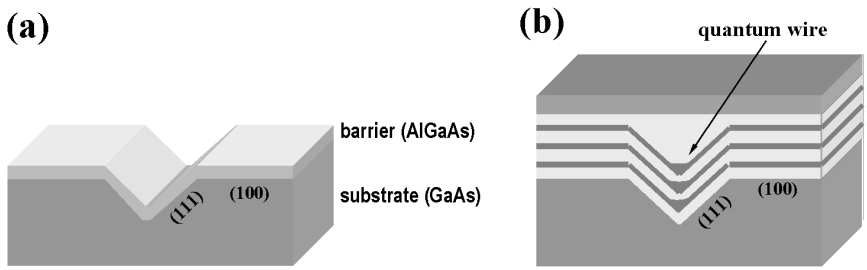

3.4.1 V-groove quantum wires

Selective growth on pre-patterned V-groove substrates, as originally developed by Kapon and co-workers [85–86], has been a popular method to fabricate nanoscale quantum wire active medium beyond the lithographic resolution [1, 87–94]. *In situ* quantum wire growth on V-groove substrates generates minimum defect densities and allows the formation of vertical stacks of identical quantum wires. Figure 12 is a schematic illustration of V-groove GaAs quantum wires (Figure 12(b)), fabricated by growing successive layers of GaAs and AlGaAs on V-grooves. The grooves are formed by wet etching into a (100) oriented GaAs substrate, a process that exposes (111)A sidewalls (Figure 12(a)). The underlying mechanism of growing quantum wires on V-grooves is the use of differences in surface migration of reactive species (e.g., group-III atoms) on different growth planes. For instance, the surface migration of a Ga atom is typically higher on the (111)A planes than on the (100) planes. This migration difference leads to a higher growth rate of GaAs on (100) planes as compared to (111)A planes, leading to a thin quantum well on the (111)A side walls and a significantly thicker quantum well at the bottom of the V-groove. Accumulation of GaAs occurs in the bottom of the groove, and hence the formation of a crescent-shaped quantum wire along the direction of the V-groove. Additionally, the surface migration for Al on the (111)A planes is lower than that for Ga atom, therefore AlGaAs growth is faster on the (111)A planes. The growth of stacked wires is therefore possible by alternating the AlGaAs and GaAs growth.

3.4.2 Λ-ridge quantum wires

Crescent quantum wires can be fabricated not only in the bottoms of V-shape grooves, but also on the ridge top by first growing a facet structure with a sharp ridge using lithography [95–98]. For example [96], GaAs quantum wires have been fabricated by growing successive layers a GaAs well on the top of the ridge structure as depicted in Figure 13. The fabrication process starts by etching the substrate to form a mesa stripe, followed by epitaxial growth of GaAs on the top of the mesa stripe to form a narrow ridge with two (111)B adjacent surfaces (Figure 13(a)). An AlAs barrier layer is deposited on the top of the ridge before a GaAs quantum well is grown to form one-dimensional quantum wire structure (Figure 13(b)).

Figure 13 Selective growth of quantum wires on a pre-patterned Λ-ridge substrate

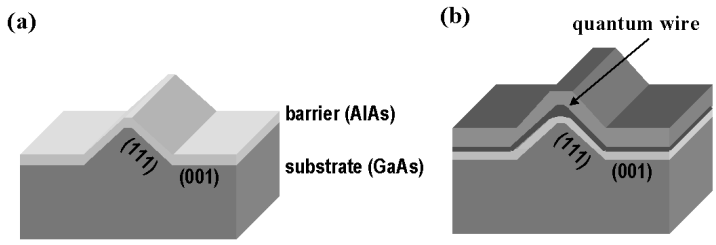

3.4.3 T-intersection quantum wires

Other than pre-patterned non-planar substrates, one-dimensional quantum wires can be formed at the T-intersection [99] of two parent quantum wells by cleaved-edge overgrowth, with two deposition (e.g., MBE) steps separated by *in situ* wafer cleaves. At the T-intersection of two quantum wells, quantum confinement of carriers forms a quantum wire. This type of T-shape quantum wires, as first proposed by Chang and co-workers [99], has been a useful nanoscale structure for the study of one-dimensional excions [100]. The cleaved-edge overgrowth method, developed around 1990, enables one to combine two thin film growth processes in two different directions to define quantum wires [101–105]. Lasing action in T-intersection quantum wires by optical pumping [106] and current injection [107] were both demonstrated. Figure 14 illustrates schematic growth steps of a single T-intersection quantum wire structure. For quantum wires grown on a (001) GaAs substrate using MBE, for example, a quantum well sandwiched between two barriers is successively grown on the substrate in the first MBE process (Figure 14(a)). Subsequently, the wafer was cleaved in the MBE chamber (Figure 14(b)), and the second quantum well with barriers was grown on the newly exposed (110) edge (Figure 14(c)).

3.5 Chemical synthesis

Over the past decade, there has been tremendous progress in chemical synthesis techniques for growing nanoscale semiconductor quantum wires (one-dimensional nanowires). As originally proposed by Wagner in 1964 [108] for Au-catalyzed Si whisker growth, a unique gas-phase reaction technique based on the so-called vapor-liquid-solid process has resulted in high quality lasing nanowires. In a typical vapor-liquid-solid process, one-dimensional anisotropic crystal growth is promoted by the presence of a liquid alloy-solid interface. A nanoscale catalyst liquid alloy droplet, which defines the diameter of the resulting one-dimensional nanostructure, serves as the preferential site for reactant adsorption and nucleation when supersaturated. The key feature of this vapor-liquid-solid process is that equilibrium phase diagrams can be applied to help select catalysts and predict growth conditions. Ideally the catalyst (e.g., Au) and the desired nanowire material (e.g., InAs) form eutectic alloys, and the growth temperature can be chosen between the eutectic point and the melting point of the nanowire material.

Figure 14 Formation of one-dimensional T-intersection quantum wire structure by cleaved-edge overgrowth

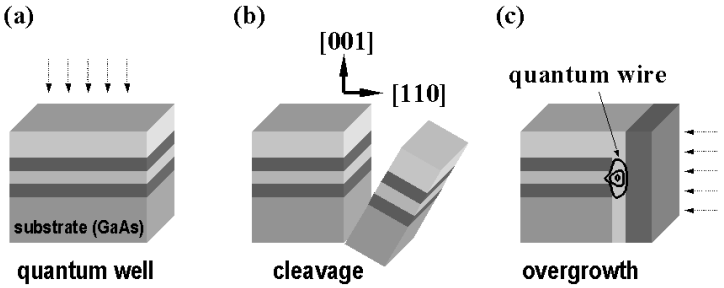

An example of the basic processing steps [109] for Au-catalyzed InAs nanowire growth is illustrated in Figure 15. The first step involves deposition of one monolayer of Au on an InAs (111)B substrate, followed by annealing that results in the formation of nanometer size Au-In liquid alloy droplets at a temperature above the Au-In eutectic point (Figure 15(a)). With trimethylindium (TMI) and arsine (AsH_3) as the source gases flowing through the liquid alloy droplets, InAs crystals precipitate at the nanoscale droplet-solid interfaces, forming long whisker-like nanowires (Figure 15(b)).

Figure 15 Catalyzed growth of nanowires through the vapor-liquid-solid process

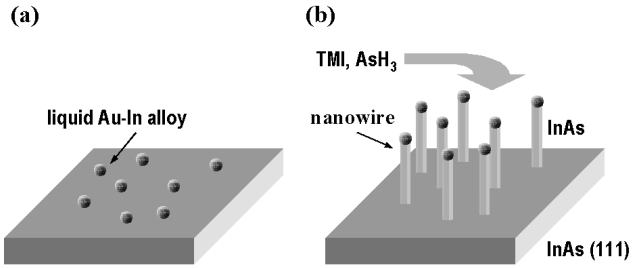

The vapor-liquid-solid process has been exploited to synthesize nanoscale semiconductor quantum wires of different compositions [110–111], including the conventional III–V (InAs, GaAs, GaP, InP) and II–IV systems (ZnS, ZnSe, CdS, CdSe), oxides (ZnO, MgO, SiO_2), nitrides (GaN), as well as elemental semiconductors (Si and Ge). Different gas sources such as chemical vapor deposition [112] and laser evaporation [113–114] have been applied to supply material species during nanowire growth. Analogy to the vapor-liquid-solid process, a solution-liquid-solid mechanism for the growth of group III–V (InP, InAs, and GaAs) semiconductor nanowires has been developed [115] based on low-temperature solution-phase reactions. Other promising chemical synthetic methods that have been employed to produce semiconductor nanowires include template-directed synthesis [116–117], aqueous precipitation [118], and solvo-thermal chemistry [119].

4 Semiconductor lasers based on one-dimensional nanostructures

The desire to realize semiconductor lasers with great color range, high material gain, and low lasing threshold has been one of the primary motivations to investigate

one-dimensional quantum wires. In 1989, Kapon and co-workers [1] first reported the observation of lasing action of quantum wires (GaAs) imbedded in a conventional diode laser cavity structure. Since then, substantial efforts have been devoted to the improvement of quantum wire laser performance as well as the realization of lasing action in various one-dimensional nanostructures incorporated in different optical cavities (Section 1.1). In later 2000, using chemically synthesized crystalline nanowires grown by Yang's group, Mao and co-workers [2] performed the first experiment that demonstrated lasing action in freestanding quantum wires (ZnO nanowires). Without imbedding into any fabricated optical cavities, lasing in nanowires is originated from simultaneous carrier and photon confinement by the one-dimensional nanoscale wire cavity. This demonstration indicates that individual quantum wires could act as both a one-dimensional active gain medium and a nanoscale optical cavity that creates a positive optical feedback.

Starting with an introduction of the early development of semiconductor lasers – from *p-n* junction lasers to quantum well lasers, this section provides a review of recent progress of semiconductor lasers based on various one-dimensional quantum wire structures. Kapon has written an excellent review [37] of early quantum wire laser research before 1992.

4.1 Semiconductor lasers – from p-n *junction to quantum wells*

Shortly after the successful operation of a solid-state ruby laser [120] in 1960, it was realized [38,121] that, in order to achieve stimulated emission from a semiconductor material, the electron and hole populations within the active region must be large enough that their quasi-Fermi levels are separated by energies greater than that of the radiation. In 1962, the first GaAs based *p-n* junction semiconductor laser was demonstrated [122–125], although this simple homojunction device was a long way from realizing practical applications. Figure 16(a) illustrates the energy band of a typical *p-n* junction semiconductor gain medium that uses heavily doped *p* and *n* regions on either side of a junction. After the injection of carriers, the area near the junction has a high density of electrons and holes simultaneously. Stimulated emission takes place in the junction region due to radiative electron-hole recombination. Lasing occurs when the rate of stimulated emission exceeds the rate of total optical losses of the laser structure.

There are several disadvantages in *p-n* junction type lasers. Since the injected carriers are free to diffuse, the spatial distribution of recombination is diluted. There is also little guiding and confinement of the electromagnetic wave being amplified in the laser cavity. In 1963, Kroemer [126–127] suggested that a double heterostructure could be used to produce an efficient semiconductor laser, an idea proposed independently by Alferov [128]. In such double heterostructure semiconductor lasers, charge carriers are concentrated and recombine in a narrow band-gap layer between two slabs of wider band-gap material (Figure 16(b)). The heterostructure also acts to confine the photons, which allows the stimulated emission to build up into a laser beam. By 1970, semiconductor lasers had advanced to where the first room temperature continuously operating heterostructure (AlGaAs/GaAs) lasers were reported [129–131]. In the process of double heterostructure laser development, Alferov [132] contributed the idea of using AlGaAs/GaAs as the key heterostructure materials, which have close values of the lattice constants thus little strain and small density of traps in the interface.

Figure 16 Schematic energy band diagrams of (a) a *p-n* junction laser, (b) a double heterojunction laser, (c) a quantum well laser and (d) a quantum cascade laser based on interminiband transitions

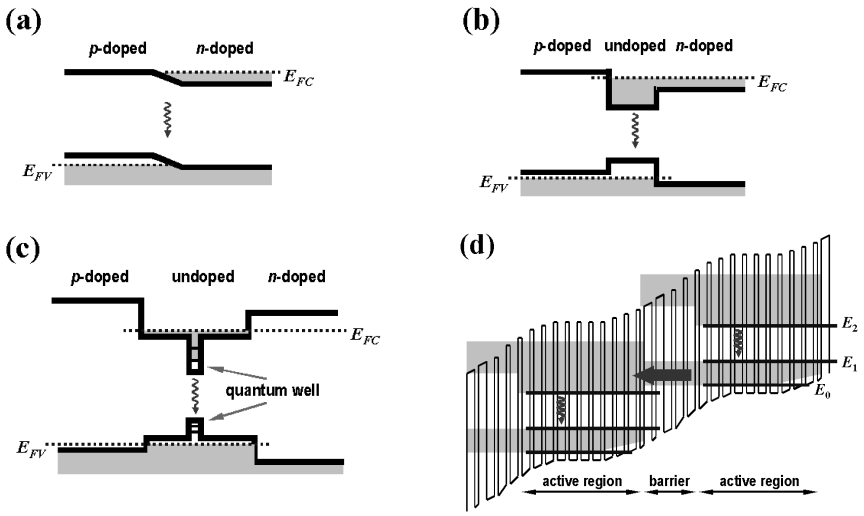

Further development of semiconductor lasers led to the realization of using quantum wells as the active gain media. As mentioned before, quantum well lasers represent the first generation of semiconductor lasers utilizing quantum size effects of a nanoscale dimension (in the direction of the quantum well thickness). In a quantum well structure, a series of energy levels and associated subbands are formed due to quantization of carriers in the direction of quantum well thickness. The carrier confinement and its resulting density of states in quantum wells promise more efficient lasing devices operating at lower lasing threshold than those with 'bulk' double heterostructure active media. Shortly after the demonstration of quantum effects in the optical spectra of a quantum well heterostructure [133], lasing in quantum well structures was accomplished in 1975 [134], followed by the construction of a quantum-well laser with parameters to match those of standard double heterostructure lasers [135]. As illustrated in Figure 16(c), stimulated recombination of electron-hole pairs takes place in the quantum well region, where the confinement of carriers and the optical mode enhance the interactions between the carriers and the radiation.

What marks a turning point in the development of quantum well lasers is the demonstration of significant reduction in lasing threshold by incorporating a quantum-well structure into the active region of a VCSEL structure [6,42,136–137]. Further performance improvements were reported by using graded heterojunction interfaces into the monolithic epitaxial distributed Bragg reflectors of the VCSEL to reduce the electrical resistance [138–139]. Additionally, microdisk lasers with quantum wells as the active media have also been fabricated, and low lasing threshold was achieved [140–144].

Yet another remarkable use of two-dimensional quantum well structures is the realization of lasing due to intersubband or interminiband transition, known as quantum cascade lasers [145–146] originally proposed in 1971 [147]. What primarily distinguishes the quantum cascade lasers from conventional semiconductor lasers [148–149] is the light generation scheme that allows one to achieve very high power by recycling many times (equal to the number of cascaded stages in a quantum cascade laser) the electrons

making the optical transition. The original quantum cascade lasers [145] rely on transitions between quantized conduction band excited states (intersubband transitions) of double quantum wells. The population inversion between the states of laser transition is designed by reducing the final state lifetime using resonant optical phonon emission. Alternatively, the quantum cascade laser can be constructed based on optical transitions (interminiband transitions) between the energy bands of superlattices – periodic stacks of nanometer-thick quantum wells, in which superimposed potentials split the conduction and valence bands into a series of narrow minibands (–100 meV) separated by energy gaps (minigaps) of comparable value [146]. A portion of the energy diagram of an interminiband cascade laser under operating bias is shown in Figure 16(d), electrons are injected into the lowest lying superlattice states of the upper miniband (E_2), where they emit a photon and relax to the highest lying superlattice states of the lower miniband (E_1). Electrons then quickly escape to the ground state (E_0) of the lower miniband by emitting optical phonons. The very short lifetime for phonon emission compared to the lifetime for interminiband transition makes it possible to maintain a population inversion. Eventually, electrons tunnel into the next active region, and typically 25 or more active regions are 'cascaded' to provide enough gain to achieve efficient lasing action. In contrast to conventional quantum well lasers, the wavelength of quantum cascade lasers is essentially determined by quantum confinement, i.e., by the layers' thickness of the active region rather than by the band-gap of the material. As such, the wavelength can be tailored over a very wide range using the same active material [148–149].

Beyond the accomplishments of the quantum well lasers that use two-dimensional nanostructures as the active gain media, the capability of growing one-dimensional quantum wires offers an additional degree of freedom in the design of semiconductor lasers. Both optically and electrically pumped semiconductor lasers have been achieved using nanoscale quantum wires as the active gain media. Since the initial demonstration of lasing from a V-groove quantum wire embedded in a micron size edge-emitting optical cavity [1], semiconductor lasers based on one-dimensional nanostructures have evolved to truly one-dimensional nanolasers – individual nanowires can act as both the gain medium and the optical cavity [2]. Semiconductor lasers based on one-dimensional quantum wires fabricated using different growth techniques will be reviewed in the following sections, which include lasing from lithographically defined, self-organized, selectively grown, and chemically synthesized nanoscale quantum wires.

4.2 Lasing from lithographically defined quantum wires

Lasing from etched quantum wires showing one-dimensional carrier confinement in its spectrum [150] was reported around 1990 after years of efforts aimed at reducing the lateral dimensions of the etched wire structures [151]. Over the past 10 years, significant performance improvements [63–65,152–155] of semiconductor lasers with the litho-graphically etched quantum wires as the active gain media have been achieved, for instance, by using a much slower growth rate than conventional deposition processes. In particular, low damage etched and re-grown interfaces have been fabricated by adopting a strain-compensated multiple quantum well structure as an initial wafer to suppress strain relaxation due to the large lattice mismatch along vertical structure [154]. Figure 17(a) is a schematic illustration of a low damage GaInAsP quantum wire laser cavity grown on a *p*-type InP (100) substrate [63,154]. The structure was fabricated by first growing a quantum well layer by MOCVD, then using reactive ion etching to form a

wire pattern in the active region through an electron-beam written mask, followed by a second MOCVD re-growth step. The cavity mirrors were cleaved such that light propagated normal to the grating grooves. The laser structure consisted of a *p*-type InP buffer layer (2 μm), an undoped $Ga_{0.22}In_{0.78}As_{0.47}P_{0.53}$ lower optical confinement layer (170 nm, lattice matched to InP), five undoped $Ga_{0.22}In_{0.78}As_{0.82}P_{0.18}$ compressively strained quantum well layers (7 nm) sandwiched using six undoped $Ga_{0.25}In_{0.75}As_{0.50}P_{0.50}$ tensile-strained barrier layers (9 nm thick), an upper optical confinement layer (45 nm) with the same composition as the lower one, and an InP cap layer (10 nm).

Figure 17 (a) Schematic illustration of an etched mesa quantum wire laser structures, (b) Cross-sectional SEM image of the active region of an etched quantum wire laser (43 nm wide quantum wires) and (c) Room temperature light output vs. current characteristics of two lithographically etched quantum wire lasers (with 43 and 70 nm wide quantum wires), and of a quantum well laser prepared on the same wafer. (After references [63] and [154])

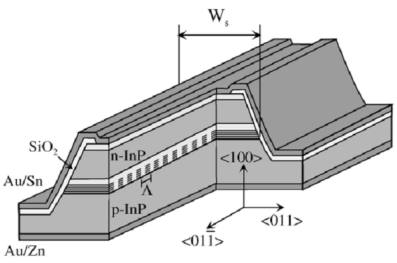

(a)

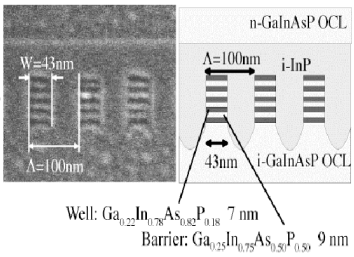

(b)

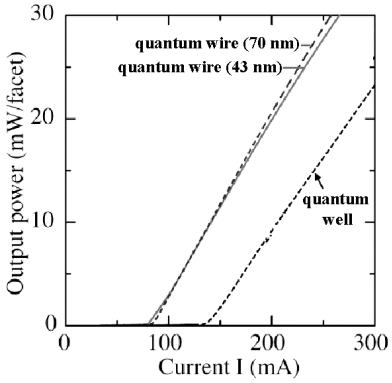

(c)

Also shown in the above figure (Figure 17(b)) is the cross-sectional SEM view around the quantum wire active region, which has a period of about 100 nm and wire width 43 nm. With respect to the lasing wavelength of a quantum well laser (λ = 1577 nm) fabricated on the same substrate, 27 meV blue-shift (λ = 1524 nm) was measured for the 43 nm quantum wire laser. As shown in Figure 17(c), the room temperature threshold current of the quantum wire laser was about 80 mA, corresponding to a current density approximately 300 A/cm^2, lower than that for the quantum well laser of the similar cavity structure. Further reduction of threshold current density, as low as 94 A/cm^2, was accomplished for a 1.5 μm wavelength GaInAsP distributed feedback laser structure consisting of two layers of periodic quantum wire active region [156].

4.3 Lasing from self-organized quantum wires

4.3.1 SILO quantum wire lasers

Substitution of a quantum well with a short period superlattice structure can create a self-organized quantum wire array with lateral composition modulation. Quantum wires grown by such strain-induced lateral ordering scheme have been applied to serve as the active media for semiconductor lasers [72,157–159].

Figure 18 (a) Schematic illustration of an edge-emitting semiconductor laser with SILO quantum wires as the active gain media. (b) Cross-sectional TEM image of the active region of a GaInAs SILO quantum wire laser. (c) The light output vs. current characteristics of two SILO quantum wire lasers operated at 77 K. The contact stripe was aligned either perpendicular ([110] emission) or parallel ([–110] emission) to the quantum wire array. (After references [72] and [159])

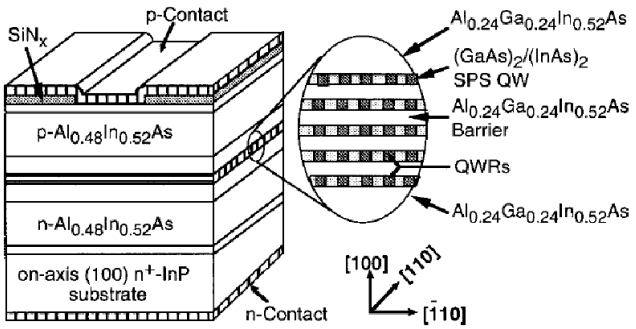

(a)

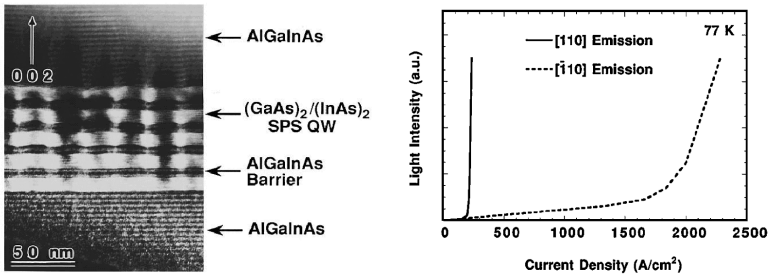

(b) (c)

Figure 18 shows a quantum wire laser based on strain-induced lateral ordering [72,159] with a 60 μm wide and 500 μm long edge-emitting cavity fabricated by MBE. The GaInAs quantum wire laser structure (Figure 18(a)), grown on a *n*-type InP (100) substrate, consists of 15 pairs of *n*-type $Ga_{0.47}In_{0.53}As/Al_{0.48}In_{0.52}As$ (5 nm/10 nm) superlattice buffer layer, a *n*-type $Al_{0.48}In_{0.52}As$ cladding layer (1 μm), an undoped active region sandwiched between an undoped $Al_{0.24}Ga_{0.24}In_{0.52}As$ lower and upper wave guiding layer (130 nm), a *p*-type $Al_{0.48}In_{0.52}As$ cladding layer (1 μm), and a *p*-type $Al_{0.47}In_{0.53}As$ cap layer. The active region consists of five quantum wells, each has 8 pairs of $(GaAs)_2/(InAs)_2$ short period superlattice layers with a total thickness of about 10 nm.

The barrier consists of a 7.5 nm $Al_{0.24}Ga_{0.24}In_{0.52}As$ layer. The strain-induced lateral ordering process occurs within the active region and strong in-plane Ga/In lateral composition modulation is spontaneously formed in the [110] direction. The sandwiched In-rich regions by the higher band-gap Ga-rich regions along the [110] direction combined with the barriers on top and bottom form an array of quantum wire heterostructure. Lasing spectra were measured at 77 and 300 K under pulsed excitation.

Figure 18(b) is the cross-sectional TEM image of the active region, strong dark and bright fringes due to composition modulation can be seen in the cross section of the $(GaAs)_2/(InAs)_2$ short period superlattice. The bright fringes correspond to the In-rich and the dark fringes correspond to the Ga-rich regions, both are 15 nm wide. The light-output versus current characteristics for two SILO quantum wire lasers with different contact strip orientations at 77 K temperature are shown in Figure 18(c). The threshold current density for laser emission in the [110] direction, which is perpendicular to the quantum wires, is significantly smaller than the case when laser emission is parallel to the quantum wires. The strong anisotropy observed in the threshold current density can be attributed to the direction of light propagation within the cavity with respect to the direction of the quantum wires. The effect of anisotropy of the electronic dipole moment in one-dimensional quantum wire lasers has been theoretically investigated [160].

Further investigations of quantum wire lasers based on strain-induced lateral ordering have shown temperature stabilized lasing and gain spectra. Both the rates for lasing wavelength shift and for gain peak wavelength shift were found [159] stable to approximately 1 Å/K, a value much smaller than the quantum well case. This temperature stability was attributed to a temperature-stabilized band-gap in the quantum wires.

4.3.2 Vicinal quantum wire lasers

Self-organization of quantum wires on vicinal multiatomic steps is an attractive technique since it does not involve post growth processing, therefore can potentially yield quantum wire structures of high interface quality without lithography induced damages. Semiconductor lasers using quantum wires self-organized on vicinal steps were demonstrated shortly after Kapon's report of the first V-groove quantum wire laser [161–164]. Figure 19(a) is a schematic illustration of a quantum wire edge-emitting laser structure using self-organized growth on vicinal GaAs multiatomic steps [165]. The InGaAs quantum wire active layer was grown on a vicinal GaAs (001) substrate, misoriented by 5° towards the [–110] direction. To form coherent GaAs multiatomic steps after the growth of a *n*-type AlGaAs cladding layer (320 nm), *n*-type $(GaAs)_2/(AlAs)_1$ superlattice buffer layers with monoatomic steps were deposited prior to the growth of GaAs multiatomic steps. The average thickness of the InGaAs layers (0.15 In content) on the GaAs multiatomic steps was 3 nm, and the average step height and period were 6.1 and 70 nm, respectively. After the growth of the InGaAs quantum wires and an undoped GaAs and a *p*-type AlGaAs cladding layer on the top of the quantum wire layer, a standard Fabry-Perot cavity was formed with cleaved facet mirrors. The cavity length was 600 μm, and its direction was in either [110] or [–110] directions, where the [110] direction is parallel to the quantum wires and the multiatomic steps, and the [–110] direction perpendicular to the quantum wires.

Figure 19 (a) Schematic illustration of a vicinal quantum wire laser structure, with InGaAs quantum wires grown on a GaAs vicinal substrate. (b) A typical AFM image of an InGaAs surface grown on GaAs multiatomic steps. (c) The 77 K lasing output vs. current characteristics of two vicinal quantum wire lasers with emission parallel and perpendicular to the quantum wires, and of a quantum well laser grown under similar fabrication conditions. (After reference [165])

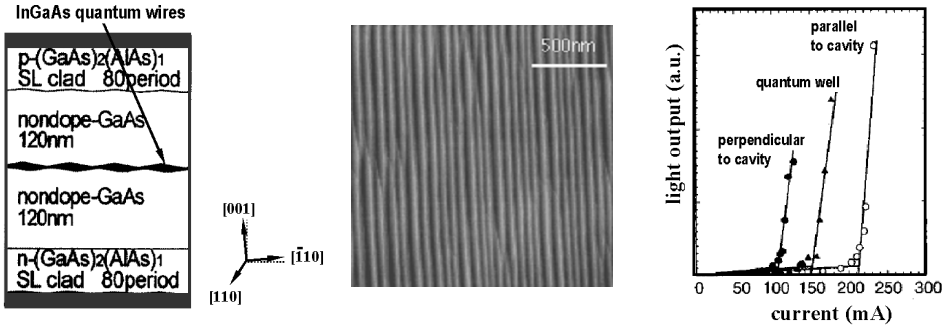

(a) (b) (c)

Figure 19(b) is a typical atomic force microscopy image of the InGaAs quantum wire structures grown on multiatomic steps of a 5° misoriented GaAs (001) substrate. Figure 19(c) shows the lasing behaviors, through pulsed current injection at 77 K, of three lasers – two vicinal InGaAs quantum wire lasers emitting parallel and perpendicular to the quantum wires and an InGaAs quantum well laser fabricated under the same grown conditions but without substrate misorientation. Threshold currents of the quantum well laser and the quantum wire lasers with cavity parallel and perpendicular to the wire array direction were approximately 150, 212 and 105 mA, respectively. These current values correspond to threshold current densities of 83, 118 and 58 A/cm^2, respectively. Clearly, minimum threshold current density was obtained for the quantum wires perpendicular to the light propagation (electric field vector parallel to the axis of the quantum wire). In terms of lasing wavelength, however, a red shift of the emission wavelength (instead of blue shift for quantum confinement) with respect to the reference quantum well laser was observed. This phenomenon was attributed to the change of composition of the locally thick InGaAs quantum wires at the edge of GaAs multiatomic steps.

Instead of simply growing a layer of quantum wires on a tilted substrate, quantum wire lasers with fractional superlattice layers grown on vicinal surfaces were also demonstrated [164]. This type of quantum lasers may have better performance due to the benefit of the fractional superlattice layers that have additional compositional modulation perpendicular to the growth direction, thus less sensitive to small variations in deposition rates. Incorporation of fractional superlattice quantum wires, grown on vicinal misoriented GaAs (001) substrates, into microcavities (VCSEL) has resulted in room temperature lasing under optical pumping [83,166]. Additionally, room temperature lasing from semiconductor lasers based on quantum wires grown on corrugated vicinal (775)B GaAs substrates and using a graded refractive index separate confinement heterostructure [82] and a VCSEL [167] were reported.

4.4 Lasing from selective grown quantum wires

4.4.1 V-groove quantum wire lasers

Since Kapon [1] reported the first observation of stimulated emission in quantum wires using V-groove structures, various types of semiconductor lasers based on V-groove quantum wires have been reported [89–90,168–173], including lasers based on a single V-groove quantum wire such as single wire AlGaAs/GaAs lasers [168] and single wire InGaAsP/InP lasers [171]. Low operation threshold at room temperature has also been achieved by improving optical gain and minimizing electrical and optical losses using, for example, a short-period V-groove quantum wire array with sub-micron dielectric current blocking [90], or a V-groove quantum wire distributed feedback cavity structure [172], or strained V-groove quantum wires and large index changes that enhance optical confinement factor and band edge density of states [169].

Another advancement of V-groove quantum wire lasers is the demonstration of lasing from the ground one-dimensional subband transition [173–174] in vertically stacked AlGaAs/GaAs multiple quantum wires. Because of small optical confinement factor as well as structural imperfections, typical quantum wire lasers require a relatively high carrier density to reach threshold, resulting in lasing from the higher subbands or the excited states of the quantum wires rather than the ground states. Ground state lasing is important in order to exploit the advantages of one-dimensional nanostructures, since quantum confinement is best manifested at the ground subbands as the excited subbands mix the motion of carriers in directions perpendicular to the axis of the wire.

Figure 20(a) shows a schematic structure of a MOCVD grown V-groove quantum wire laser [94] with a SiO_2 current blocking configuration. The V-grooves aligned along the [01-1] direction with a period of 4 μm were formed on a (001) GaAs substrate by wet chemical etching. The laser structure consists of a *n*-type GaAs buffer layer (0.3 μm), a *n*-type $Al_{0.5}Ga_{0.5}As$ lower cladding layer (1 μm), an undoped $Al_{0.2}Ga_{0.8}As$ guiding layer (0.2 μm), three GaAs quantum wires (8 nm) separated by two undoped $Al_{0.2}Ga_{0.8}As$ barrier layers (25 nm), an undoped $Al_{0.2}Ga_{0.8}As$ guiding layer (0.2 μm), a *p*-type $Al_{0.5}Ga_{0.5}As$ upper cladding layer (1 μm), and a *p*-type GaAs contact layer (0.2 μm). After the growth, the sidewall and the top of the quantum wire laser structure were etched out in order to improve the carrier-injection efficiency. A 100 nm SiO_2 film was deposited using ion-beam sputtering on the etched surface for current confinement, leaving a 0.5 μm wide opening for current feeding.

Figure 20(b) is the TEM cross-sectional image of three vertically stacked quantum wires. Each of the crescent-shape V-groove quantum wire is 8 nm thick at the center. Figure 20(c) shows the pulsed output lasing power versus injection current at different temperatures for a V-groove quantum wire laser with a length of 300 μm. The rate of increase of the threshold current as a function of temperature is about 0.033 mA/K. Figure 20(d) is the low-temperature (4.5 K) photoluminescence (PL), photoluminescence excitation (PLE), and lasing spectra, with the PLE spectra measured by exciting the quantum wire laser structure normal to the wafer plane with two different linear polarization directions. The broad PL/PLE peak at 1.584 eV (782.8 nm) was attributed to the lowest lying electron and heavy-hole-like states; the emission wavelength of the quantum wire laser virtually coincides with this PL/PLE peak. This agreement between the lasing wavelength and the PL peak was found to hold at higher temperatures (up to 230 K), possibly can be extended to room temperature.

Figure 20 (a) Schematic illustration of a V-groove quantum wire laser. (b) A cross-sectional TEM image of three V-groove quantum wires. (c) Light output vs. current characteristics for pulsed operation of an AlGaAs/GaAs V-groove quantum wire laser at temperatures between 10°C and 70°C. (d) Low temperature photoluminescence (PL), photoluminescence excitation (PLE), and lasing spectra of a V-groove quantum wire laser. The photoluminescence peak positions are consistent with the lasing wavelengths. (After reference [94])

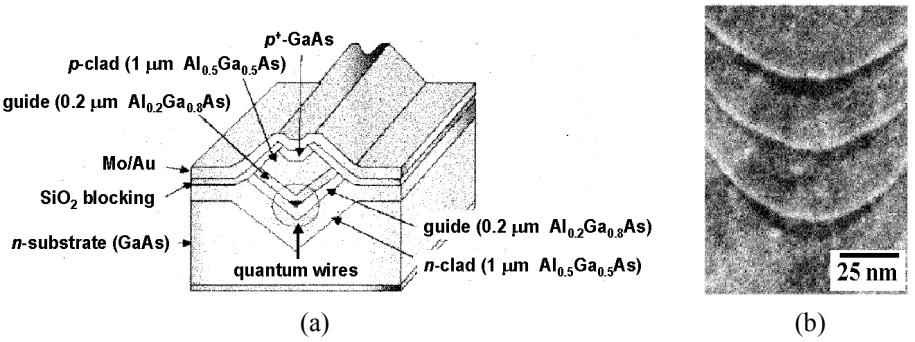

(a) (b)

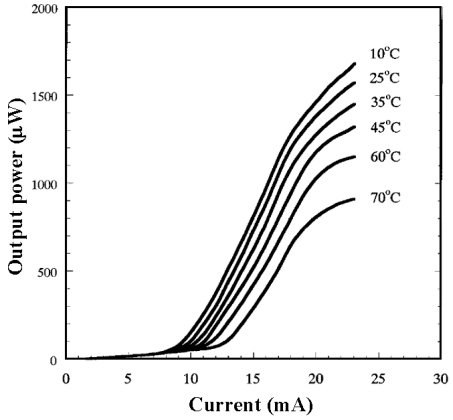

(c)

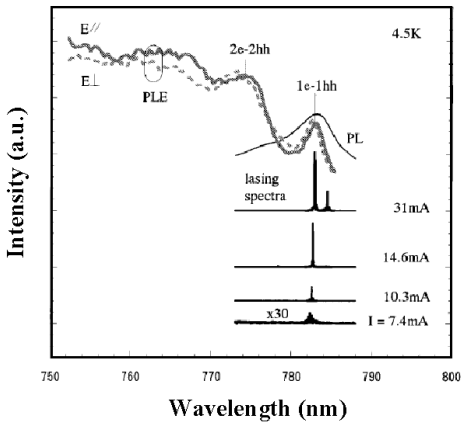

(d)

Figure 21 (a) Schematic illustration of a ridge quantum wire laser. (b) Cross-sectional TEM image of a ridge quantum wire laser active region. (c) Lasing spectra of a Λ-ridge quantum wire laser at 77 K for different optical pumping power. (After reference [175])

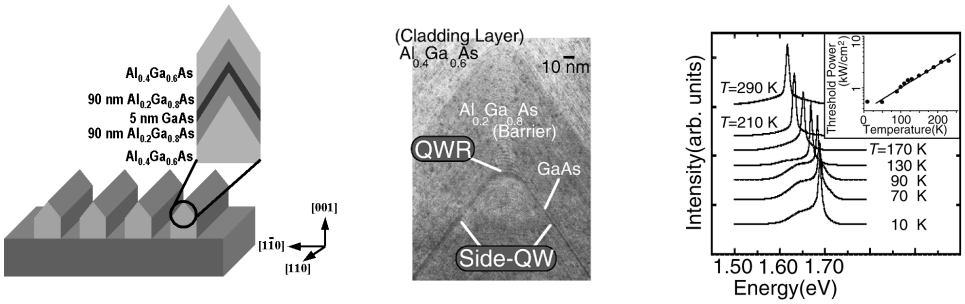

(a) (b) (c)

4.4.2 Λ-Ridge quantum wire lasers

Similar to V-groove quantum wire lasers, lasing action by optical pumping in Λ-ridge quantum wire structures has also been reported [175–176]. The ridge quantum wire structure may have the advantage of easily achieving large lateral carrier confinement at its ridge-air interface. Figure 21(a) shows a schematic structure [175] of a MBE grown Λ-ridge quantum wire laser. The Λ-ridges with a period of 4 μm were formed on a patterned (001) GaAs substrate with reverse mesa stripes running along the [110] direction. The laser structure consists of an $Al_{0.4}Ga_{0.6}As$ lower cladding layer, an $Al_{0.2}Ga_{0.8}As$ lower barrier layer (90 nm), a GaAs active quantum wire layer (5 nm), an $Al_{0.2}Ga_{0.8}As$ upper barrier layer (90 nm), and an $Al_{0.4}Ga_{0.6}As$ upper cladding layer. The curvature of the ridge top has a lateral width of approximately 10 nm. After the MBE growth, the sample was cleaved into 300 μm in length to form an optical cavity. Figure 21(b) is a cross-sectional TEM image of a ridge quantum wire laser active region.

Figure 21(c) shows the temperature dependence of lasing spectra. Optical excitation was performed by the second harmonics of mode-locked yttrium-lithium fluoride (YLF) laser pulses with a wavelength of 526 nm and pulse duration of 50 ps, incident on the top of the ridge structures. Lasing action was observed at temperatures between 4.7 and 290 K, and the peak wavelength corresponds to the transition from excited subbands of the quantum wires. The lasing energy became gradually lower at higher temperatures, which was considered to result from temperature dependence of the band-gap energy. The temperature dependence of the threshold pump power for stimulated emission was given in the inset of Figure 21(c).

4.4.3 T-intersection quantum wire lasers

Since the first demonstration of optically pumped lasing from ground quantum wire states using multiple T-intersection quantum wires [106], significant development have been achieved in the realization of semiconductor lasers based on T-intersection quantum wires by cleaved edge overgrowth method [107,177–178]. Notably, the first current injection T shape quantum wire laser was reported in 1994 [107], and recently, a single T-intersection quantum wire was seen to exhibit lasing action from ground state subband by optical pumping [178].

Figure 22 (a) Schematic illustration of a T-intersection quantum wire laser. (b) Light output vs. current characteristics for two T-intersection quantum wire lasers. (c) Current dependent lasing spectra of a T-intersection quantum wire laser. (After reference [107])

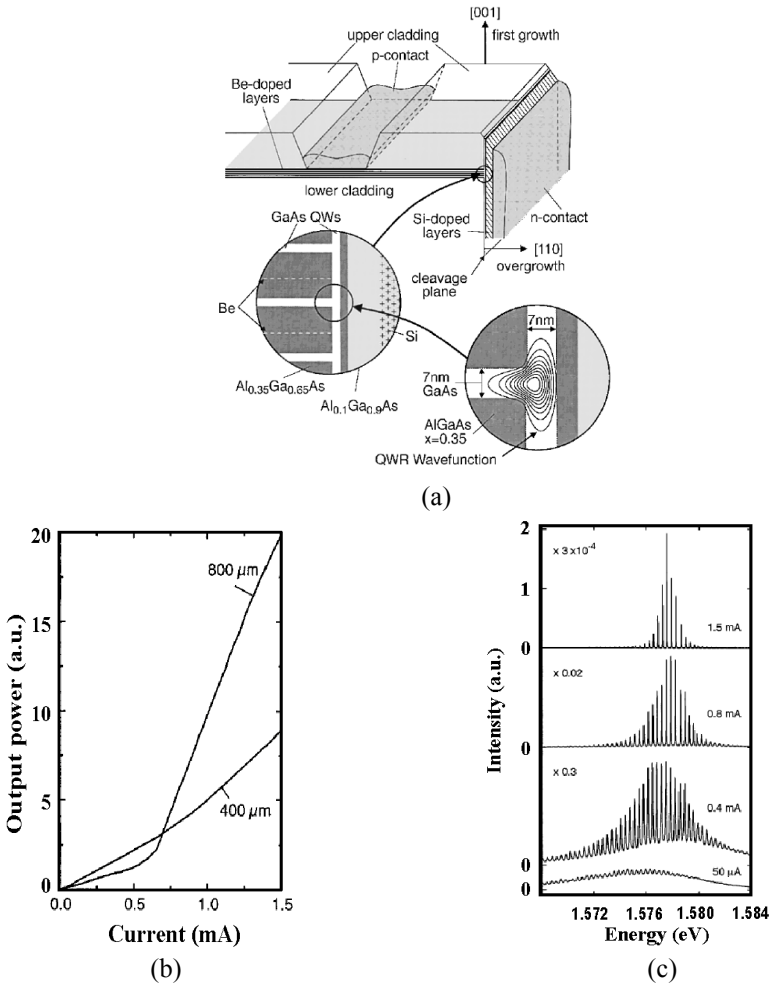

A schematic view of a current injection T-intersection quantum wire laser structure [107] is shown in Figure 22(a). The first MBE growth on a [001] GaAs substrate consists of a GaAs buffer layer (0.5 μm), an $Al_{0.5}Ga_{0.5}As$ lower cladding layer (1 μm), a 15-period *p*-type GaAs/$Al_{0.35}Ga_{0.65}As$ multiple quantum well structure (with well and barrier thickness of 7 and 58 nm), an $Al_{0.5}Ga_{0.5}As$ upper cladding layer (3 μm), and a GaAs cap layer (10 nm). The overgrowth along the [100] direction consists of an undoped GaAs quantum well (7 nm) followed by an $Al_{0.35}Ga_{0.65}As$ barrier (7 nm), an $Al_{0.1}Ga_{0.9}As$ wave setback layer (43 nm), a *n*-type $Al_{0.1}Ga_{0.9}As$ layer (124 nm), a *n*-type $Al_{0.5}Ga_{0.5}As$ cladding layer (1 μm), and a *n*-type GaAs cap layer (10 nm). The cladding layers (and the AlGaAs layer) serve as a T shape dielectric wave guide confining optical mode in the vicinity of the quantum wire array. Figure 22(b) shows the light-current characteristics of two T-intersection quantum wire lasers with cavity lengths of 400 and 800 mm at 4.2 K.

The 800 μm laser shows clear super linear behavior with a threshold current of less than 0.6 mA, compared to the 400 μm laser, which has a threshold current of about 0.4 mA.

The evolution of emission from T-intersection quantum wire laser with increasing current is shown in Figure 22(c). Increasing current injection levels results in progressively narrowing laser emission spectra as well as clear individual Fabry-Perot peaks. Also seen in Figure 22(c), there is no appreciable shift of the T-intersection quantum wire laser emission energy over relatively large changes in excitation levels, in contrast to GaAs/AlGaAs quantum well lasers that typically display a pronounced red shift with increasing injection current due to the carrier density dependent band-gap shrinkage. This observation was interpreted as the signature for excitonic gain in T-intersection quantum wires.

4.5 Lasing from chemically synthesized crystalline nanowires

Room temperature lasing action from chemically synthesized nanoscale ZnO quantum wires (nanowires) was recently demonstrated [2]. The ZnO nanowires were grown with a vapor-liquid-solid process via catalyzed epitaxial crystal growth (Section 3.5). Using Au as the catalysts, selective ZnO nanowire growth was achieved by patterning a thin Au film on a single crystal sapphire substrate (Figure 23(a)). Figure 23(b) shows a typical SEM image of ZnO nanowire arrays grown on a sapphire (110) substrate. The majority of nanowires have diameters between 70 and 100 nm, and lengths of about 5 μm. Due to the existence of a good epitaxial interface between the (0001) plane of the ZnO nanowire and the (110) plane of the substrate [179], nearly all of the ZnO nanowires can grow vertically from the substrate. The sapphire *a* plane (110) is two-fold symmetric, whereas the ZnO *c* plane is six-fold symmetric. They are essentially incommensurate with the exception that the *a* axis of ZnO and the *c* axis of sapphire are related almost exactly by a factor of 4, with a mismatch of less than 0.08% at room temperature. Such a coincidental lattice matching along the sapphire [0001] direction, combined with a strong tendency of ZnO to grow in the *c* orientation, leads to the unique vertical epitaxial growth configuration as seen in Figure 23(b).

Figure 23(c) and Figure 23(d) show respectively the light emission spectra and pumping dependent intensity from ZnO nanowires under room temperature optical excitation. The fourth harmonic of a solid state Nd:yttrium-aluminum-garnet laser (Nd:YAG, 266 nm, 3 ns pulse duration) was applied as the pumping source. The pump beam was focused on nanowires at an incidence angle of 10° to the symmetric axis of the nanowire. Light emission was collected in the direction normal to the end surface plane (along the symmetric axis) of the nanowires. In the absence of any intentionally fabricated mirrors, lasing action in ZnO nanowires was recorded as shown in Figure 23(c). At low pumping intensity, the optical spectrum consists of a single broad spontaneous emission peak with a full width at half maximum of ~17 nm. This spontaneous emission is 140 meV below the band-gap (3.37 eV) and may be attributed to the recombination of excitons through an exciton–exciton collision process [180–181]. As the excitation intensity exceeds a threshold (~40 kW/cm^2) at room temperature (Figure 23(d)), lasing peaks with line width approximately 0.3 nm emerge in the emission spectra. The lasing threshold is lower than that for lasing (~300 kW/cm^2) in disordered particles or thin films [182]. The observation of lasing action in these nanowire arrays without any fabricated mirror indicates that the crystalline well-faceted nanowires can act

as natural optical cavities. For ZnO nanowires grown on a sapphire substrate, one end of the nanowire is the epitaxial interface between the sapphire and ZnO, whereas the other end is the crystalline ZnO (0001) plane exposed in air. The spacing between individual longitudinal modes is about 5 nm, consistent with the cavity length of approximately 5 μm according to the expression of the free spectral range (Equation (1)).

Figure 23 (a) Schematic illustration of nanowire nanolasers grown on a sapphire substrate. (b) A SEM image of ZnO nanowire arrays. (c) Optical emission spectra for ZnO nanowire nanolasers below and above the lasing threshold. (d) Optical (266 nm) pumping energy dependent light emission intensity from ZnO nanowires at room temperature

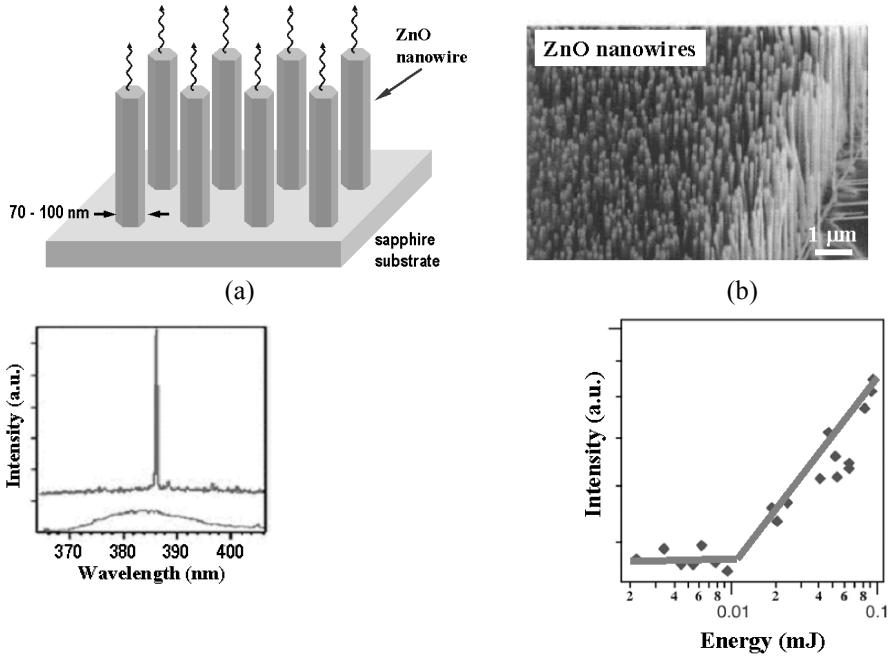

The above experiment happened to be the first demonstration of lasing of one-dimensional nanostructure without embedding the nanoscale quantum wires into any fabricated (microscale) optical cavity. The nanowire itself serves as both the active gain medium and the nanoscale optical cavity that creates a positive optical feedback. This surface-emitting nanolaser mechanism has been corroborated by near field optical spectroscopy of single nanowire lasing [183–185], and more recently, electrically pumped lasing from CdS nanowires [186].

5 Concluding remarks

5.1 Development of quantum dot lasers

In view of further scale-down of the semiconductor active gain media, impressive progress for lasers based on zero-dimensional quantum dots [187–188,31] have been

achieved recently, in parallel with the rapid development of quantum wire lasers. Additional stimulus towards the realization of quantum dot lasers comes from the prospect of quantum communication based on single photon emission [189–191] from semiconductor quantum dots. Breakthroughs in defect-free quantum dot (nanocrystal) growth techniques, especially the self-assembly method known as the Stranski-Krastanov process [192–196] and the chemical synthetic routes based on stabilized replacement reactions [197–204], have led to significant performance improvement of quantum dot lasers [205]. Other than embedding quantum dots into edge-emitting laser cavities [206], quantum dot surface-emitting lasers [207–208], quantum dot photonic crystal lasers [209], and quantum dot microdisk lasers [210–211] have all been realized. Record low threshold current densities on the order of 10 A/cm^2 [41,212] have also been reported for quantum dot lasers fabricated by MBE and MOCVD. However, the stochastic nature of the size and density of quantum dots has limited the optical gain of semiconductor lasers using quantum dots as the active gain media. One-dimensional wire-like alignment of high-density quantum dots through a combination of different growth techniques, such as the one reported recently [213], could be a possible solution.

5.2 Prospective

Miniaturization has been the subject of substantial research interest in photonics as in electronics. One major direction of contemporary semiconductor laser research is the realization of novel lasing devices that benefit from quantum confinement associated with low-dimensional (1D and 0D) semiconductor nanostructures. Dramatic progress in the development of nanoscale crystal growth and fabrication technologies has driven the miniaturization of semiconductor lasers, a trend also motivated by the desire to achieve greater color range, higher optical gain, and lower lasing threshold. The preceding sections provided a general picture of the current status of semiconductor laser technology based on one-dimensional nanoscale quantum wires, and offered an introduction to some of the essential characteristics of quantum confinement in nanoscale semiconductor materials. Semiconductor lasers using nanoscale quantum wires as the active gain media have evolved from ‘microlasers’ in which the one-dimensional nanostructure is embedded in a microscale optical cavity, to ‘nanolasers’ in which the material gain and optical feedback are simultaneously achieved by individual one-dimensional nanowires. An immediate goal for quantum wire laser development is to explore the capability of integration with electronic and photonic circuits to realize practical applications.

In fact, the realization of the nanowire nanolasers offers a potential route for achieving simultaneous lateral carrier and photon confinement. As discussed previously, when the size of an active semiconductor gain material is reduced to the nanometer scale, quantization of the transition energies and narrowing of the density of states result in lasers with great color range, high material gain, and low lasing threshold. In the mean time, although less obvious, carrier confinement in nanoscale semiconductors can lead to an increase in the exciton binding energy and the oscillator strength for radiative recombination [214–218]; photon confinement in miniature optical cavities can lead to an enhancement of the spontaneous emission rate and emission coupling to the fundamental cavity mode [219–222]. Still under intensive investigations, enhancement of the excitonic interaction and of the spontaneous emission rate in nanoscale quantum wires (and

quantum dots) may provide additional mechanisms for realizing better performance semiconductor lasers.

While quantum well lasers are maturing toward commercial applications, semiconductor lasers based on one-dimensional (and zero-dimensional) nanoscale materials are still in their early development stage. The full promise of quantum wire (and quantum dot) lasers must await advances in device optimization, which has to be based on a thorough understanding of the physics of stimulated emission from nanoscale quantum structures. The understanding of semiconductor lasers based on nanoscale quantum wires (and quantum dots) is not complete, nor is their development, which is certain to continue.

6 Acknowledgements

This research has been supported by the U.S. Department of Energy under contract No. DE-AC03-76SF00098.

References

1 Kapon, E., Hwang, D.M. and Bhat, R. (1989) *Phys. Rev. Lett*., Vol. 63, p.430.

2 Huang, M., Mao, S.S., Feick, H., Yan, H., Wu, Y., Kind, H., Weber, E.R., Russo, R.E. and Yang, P. (2001) *Science*, Vol. 292, p.1897; Mao, S.S., Russo, R.E. and Yang, P. (2001) *Proc. SPIE*, Vol. 4608, p.225.

3 Coldren, L.A. and Corzine, S.W. (1995) *Diode Lasers and Photonic Integrated Circuits*, Wiley, New York.

4 Zory Jr., P.S. (Ed.) (1993) *Quantum Well Lasers*, Academic, San Diego.

5 Verdeyen, J.T. (1995) *Laser Electronics*, 3rd ed., Prentice-Hall, Englewood Cliffs.

6 Jewell, J.L., Harbison, J.P., Scherer, A., Lee, Y.H. and Florez, L.T. (1991) *IEEE J. Quantum Electron*., Vol. 27, p.1332.

7 Soda, H., Iga, K., Kitahara, C. and Suematsu, Y. (1979) *Japan. J. Appl. Phys*., Vol. 18, p.2329.

8 Iga, K., Ishikawa, S., Ohkouchi, S. and Nishimura, T. (1984) *Appl. Phys. Lett*., Vol. 45, p.348.

9 Koyama, F., Kinoshita, S. and Iga, K. (1989) *Appl. Phys. Lett*., Vol. 55, p.221.

10 Kogelnik, H. and Shanks, C.V. (1972) *J. Appl. Phys*., Vol. 43, p.2327.

11 Lee, Y.H., Jewell, J.L., Scherer, A., McCall, S.L., Harbison, J.P. and Florez, L.T. (1989) *Electron. Lett*., Vol. 25, p.1377.

12 Huffaker, D.L., Graham, L.A., Deng, H. and Deppe, D.G. (1996) *IEEE Photon. Tech. Lett*., Vol. 8, p.974.

13 Schubert, E.F., Lu, L.W., Zydzik, G.J., Kopf, R.F., Benvenuti, A. and Pinto, M.R. (1992) *Appl. Phys. Lett*., Vol. 60, p.466.

14 Chalmers, S.A., Lear, K.L. and Killeen, K.P. (1993) *Appl. Phys. Lett*., Vol. 62, p.1585.

15 Peters, M.G., Thibeault, B.J., Young, D.B., Scott, J.W., Peters, F.H., Gossard, A.C. and Coldren, L.A. (1993) *Appl. Phys. Lett*., 63, 3411.

16 Hegblom, E.R., Babic, D.I., Thibeault, B.J. and Coldren, L.A. (1997) *IEEE J. Sel. Top. Quantum Electron*., Vol. 3, p.379.

17 Yablonovitch, E. (1987) *Phys. Rev. Lett*., Vol. 58, p.2059.

18 John, S. (1987) *Phys. Rev. Lett*., Vol. 58, p.2486.

19 Painter, O.J., Lee, R.K., Scherer, A., Yariv, A., O'Brien, J.D., Dapkus, P.D. and Kim, I. (1999) *Science*, 284, 1819.

20 Painter, O.J., Husain, A., Scherer, A., O'Brien, J.D., Kim, I. and Dapkus, P.D. (1999) *J. Lightwave Tech*., Vol. 17, p.2082.

21 Hwang, J.K., Ryu, H.Y., Song, D.S., Han, I.Y., Song, H.W., Park, H.K., Lee, Y.H. and Jang, D.H. (2000) *Appl. Phys. Lett*., Vol. 76, p.2982.

22 Hwang, J.K., Ryu, H.Y., Song, D.S., Han, I.Y., Park, H.K., Jang, D.H. and Lee, Y.H. (2000) *IEEE Photon. Tech. Lett*., Vol. 12, p.1295.

23 Song, D.S., Kim, S.H., Park, H.G., Kim, C.K. and Lee, Y.H. (2002) *Appl. Phys. Lett*., Vol. 80, p.3901.

24 McCall, S.L., Levi, A.F.J., Slusher, R.E., Pearton, S.J. and Logan, R.A. (1992) *Appl. Phys. Lett*., Vol. 60, p.289.

25 Gayral, B., Gerard, J.M., Lemaitre, A., Dupuis, C., Manin, L. and Pelouard, J.L. (1999) *Appl. Phys. Lett*., Vol. 75, p.1908.

26 Purcell, E.M. (1946) *Phys. Rev*., Vol. 69, p.681.

27 Benisty, H., Gerard, J.-M., Houdre, R., Rarity, J. and Weisbuch, C. (Eds.) (1999) *Confined Photon Systems*, Springer, Berlin.

28 Arakawa, Y. and Sakaki, H. (1982) *Appl. Phys. Lett*., Vol. 40, p.939.

29 Asada, M., Miyamoto, Y. and Suematsu, Y. (1986) *IEEE J. Quantum Electron*., Vol. 22, p.1915.

30 Nambu, Y. and Asakawa, K. (1995) *Appl. Phys. Lett*., Vol. 67, p.1509.

31 Eisler, H.J., Sundar, V.C., Bawendi, M.G., Walsh, M., Smith, H.I. and Klimov, V. (2002) *Appl. Phys. Lett*., Vol. 80, p.4614.

32 Laude, J.-P. (2002) DWDM Fundamentals, Components, and Applications, Artech, London.

33 Murray, C.B., Norms, D.G. and Bawendi, M.G. (1993) *J. Am. Chem. Soc*., Vol. 115, p.8706.

34 Efros, A.L. and Rosen, M. (2000) *Annu. Rev. Mater. Sci*., Vol. 30, p.475.

35 Brus, L.E. (1984) *J. Chem. Phys*., Vol. 80, p.4403.

36 Brus, L.E. (1986) *J. Chem. Phys*., Vol. 90, p.2555.

37 Kapon, E. (1992) *Proc. IEEE*, Vol. 80, p.398.

38 Bernard, M.G.A. and Duraffourg, G. (1961) *Phys. Stat. Sol*., Vol. 1, p.699.

39 Liu, G.T., Stintz, A., Li, H., Malloy, K.J. and Lester, L.F. (1999) *Electron. Lett*., Vol. 35, p.1163.

40 Lester, L.F., Stintz, A., Li, H., Newell, T.C., Pease, E.A., Fuchs, B.A. and Malloy, K. (1999) *IEEE Photon. Tech. Lett*., Vol. 11, p.931.

41 Eliseev, P.G., Li, H., Stintz, A., Liu, G.T., Newell, T.C., Maloy, K.J. and Lester, L. (2000) *Appl. Phys. Lett*., Vol. 77, p.262.

42 Iga, K. (2000) *IEEE J. Sel. Top. Quantum Electron*., Vol. 6, p.1201.

43 Yariv, A. (1988) *Appl. Phys. Lett*., Vol. 53, p.1033.

44 Miyamoto, Y., Miyake, Y., Asada, M. and Suematsu, Y. (1985) *IEEE J. Quantum Electron*., Vol. 25, p.2001.

45 Asada, M., Miyamoto, Y. and Suematsu, Y. (1985) *Japan. J. Appl. Phys*., Vol. 24, p.L95.

46 Alferov, Z. (2000) *IEEE J. Sel. Top. Quantum Electron*., Vol. 6, p.832.

47 Ledentsov, N.N. (2002) *IEEE J. Sel. Top. Quantum Electron*., Vol. 8, p.1015.

48 Arakawa, Y. (2002) *Trans. IEICE*, Vol. E85, p.37.

49 Ledentsov, N.N. (1999) *Semicon*., Vol. 33, p.946.

50 Cho, A.Y. (1971) *J. Vac. Sci. Tech*., Vol. 8, p.S31.

51 Cho, A.Y. (1971) *Appl. Phys. Lett*., Vol. 19, p.467.

52 Manasevit, H.M. (1968) *Appl. Phys. Lett*., Vol. 12, p.156.

53 Dupuis, R.D., and Dapkus, P.D. (1977) *Appl. Phys. Lett*., Vol. 31, p.466.

54 Panish, M.B., Temkin, H. and Sumski, S. (1985) *J. Vac. Sci. Tech*., Vol. B3, p.657.

55 Osbourn, G.C. (1982) *J. Appl. Phys*., Vol. 53, p.1586.

56 Kash, K., Scherer, A., Worlock, I.M., Craighead, H.G. and Tamargo, M.C. (1986) *Appl. Phys. Lett*., Vol. 49, p.1043.

57 Gershoni, D., Temkin, H., Dolan, C.J., Dunsmuir, J., Chu, S.N.G. and Panish, M.B. (1988) *Appl. Phys. Lett*., Vol. 53, p.995.

58 Maile, B.E., Forchel, A., Germann, R., Grützmacher, D., Meier, H.P. and Reithmaier, J.P. (1989) *J. Vac. Sci. Tech*., Vol. B7, p.2030.

59 Kohl, M., Heitmann, D., Grambow, P. and Ploog, K. (1989) *Phys. Rev. Lett*., Vol. 63, p.2124.

60 Clausen Jr., E.M., Harbison, J.P., Florez, L.T. and Van der Gaag, B.P. (1990) *J. Vac. Sci. Tech*., Vol. B8, p.1960.

61 Izrael, A., Sermage, B., Marzin, J.Y., Ougazzaden, A., Azoulay, R., Etrillard, J., Thierry-Mieg, V. and Henry, L. (1990) *Appl. Phys. Lett*., Vol. 56, p.830.

62 Notomi, M., Naganuma, M., Nishida, T., Tamamura, T., Iwamura, H., Nojima, S. and Okamoto, M. (1991) *Appl. Phys. Lett*., Vol. 58, p.720.

63 Nunoya, N., Nakamura, M., Yasumoto, H., Tamura, S. and Arai, S. (1999) *Japan. J. Appl. Phys*., Vol. 38, p.L1323.

64 Nunoya, N., Nakamura, M., Yasumoto, H., Tamura, S. and Arai, S. (2000) *Japan. J. Appl. Phys*., Vol. 39, p.3410.

65 Yagi, H., Muranushi, K., Nunoya, N., Sano, T., Tamura, S. and Arai, S. (2002) *Appl. Phys. Lett*., Vol. 81, p.966.

66 Ils, P., Michel, M., Forchel, A., Gyuro, I., Klenk, M. and Zielinski, E. (1994) *Appl. Phys. Lett*., Vol. 64, p.496.

67 Cibert, J., Petroff, P.M., Dolan, G.J., Pearton, S.J., Gossard, A.C. and English, J.H. (1986) *Appl. Phys. Lett*., Vol. 49, p.1275.

68 Zarem, H.A., Sercel, P.C., Hoenk, M.E., Lebens, J.A. and Vahala, K.J. (1989) *Appl. Phys. Lett*., Vol. 54, p.2692.

69 Hsieh, K.C., Baillargeon, J.N. and Cheng, K.Y. (1990) *Appl. Phys. Lett*., Vol. 57, p.2244.

70 Cheng, K.Y., Hsieh, K.C. and Baillargeon, J.N. (1992) *Appl. Phys. Lett*., Vol. 60, p.2892.

71 Chou, S.T., Hsieh, K.C., Cheng, K.Y. and Chou, L.J. (1995) *J. Vac. Sci. Tech*., Vol. B13, p.650.

72 Chou, S.T., Cheng, K.Y., Chou, L.J. and Hsieh, K.C. (1995) *Appl. Phys. Lett*., Vol. 17, p.2220.

73 Chou, S.T., Cheng, K.Y., Chou, L.J. and Hsieh, K.C. (1995) *J. Appl. Phys*., Vol. 78, p.6270.

74 Francoeur, S., Hanna, M.C., Norman, A.G. and Mascarenhas, A. (2002) *Appl. Phys. Lett*., Vol. 80, p.243.

75 Fetzer, C.M., Lee, R.T., Jun, S.W., Stringfellow, G.B., Lee, S.M. and Seong, T.Y. (2001) *Appl. Phys. Lett*., Vol. 78, p.1376.

76 Twesten, R.D., Follstaedt, D.M., Lee, S.R., Jones, E.D., Reno, J.L., Millunchick, J.M., Norman, A.G., Ahrenkiel, S.P. and Mascarenhas, A. (1999) *Phys. Rev*., Vol. B60, p.13619.

77 Petroff, V.M., Gossard, A.C. and Wiegmann, W. (1984) *Appl. Phys. Lett*., Vol. 45, p.620.

78 Gaines, J.M., Petroff, P.M., Kroemer, H., Simes, R.I., Geels, R.J. and English, J.H. (1988) *J. Vac. Sci. Tech*., Vol. B6, p.1378.

79 Fukui, T. and Saito, H. (1990) *Japan. J. Appl. Phys*., Vol. 29, p.L731.

80 Hara, S., Ishizaki, J., Motohisa, J., Fukui, T. and Hasegawa, H. (1994) *J. Cryst. Growth*, Vol. 145, p.692.

81 Yamamoto, M., Higashiwaki, M., Shimomura, S., Sano, N. and Hiyamizu, S. (1997) *Japan. J. Appl. Phys*., Vol. 36, p.6285.

82 Higashiwaki, M., Ikawa, S., Shimomura, S. and Hiyamizu, S. (1999) *J. Cryst. Growth*, Vol. 201, p.886.

83 Chavez-Pirson, Ando, H., Saito, H. and Kanbe, H. (1993) *Appl. Phys. Lett*., Vol. 62, p.3082.

84 Nakashima, H., Kato, T., Maehashi, K., Nishida, T., Inoue, Y., Takeuchi, T., Inoue, K., Fischer, P., Christen, J., Grundmann, M. and Bimberg, D. (1998) *Mater. Sci. Eng*., Vol. B51, p.229.

85 Kapon, E., Tamargo, M.C. and Hwang, D.M. (1987) *Appl. Phys. Lett*., Vol. 50, p.347.

86 Bhat, R., Kapon, E., Hwang, D.M., Koza, M.A. and Yun, C.P. (1988) *J. Cryst. Growth*, Vol. 93, p.850.

87 Kapon, E., Kash, K., Clausen, E.M. Jr., Hwang, D.M. and Colas, E. (1992) *Appl. Phys. Lett*., Vol. 60, p.477.

88 Percival, C., Houston, P.A., Woodhead, J., Al-Khafaji, M., Hill, G., Roberts, J.S. and Knights, A.P. (2000) *IEEE Trans. Electron Dev*., Vol. 47, p.1769.

89 Simhony, S., Kapon, E., Colas, T., Hwang, D.M., Stoffel, N.G. and Worland, P. (1991) *Appl. Phys. Lett*., Vol. 59, p.2225.

90 Kim, T.G., Park, K., Kim, E.K., Min, S. and Park, J. (1997) *IEEE Photon. Tech. Lett*., Vol. 9, p.2.

91 Kim, T.G., Suzuki, Y., Shimiz, M. and Ogura, M. (1999) *Solid State Electron*., Vol. 43, p.2093.

92 Kim, T.G., Wang, X.-L., Komori, K., Hikosaka, K. and Ogura, M. (1999) *Electron. Lett*., Vol. 35, p.639.

93 Kim, T.G., Suzuki, Y. and Ogura, M. (2000) *IEEE Photon. Tech. Lett*., Vol. 12, p.104.

94 Kim, T.G., Wang, X.-L., Suzuki, Y., Komori, K. and Ogura, M. (2000) *IEEE J. Sel. Top. Quantum Electron*., Vol. 6, p.511.

95 Koshiba, S., Noge, H., Akiyama, H., Inoshita, T., Nakamura, Y., Shimizu, A., Nagamune, Y., Tsuchiya, M., Kano, H. and Sakaki, H. (1994) *Appl. Phys. Lett*., Vol. 64, p.363.

96 Akiyama, H., Koshiba, S., Someya, T., Wada, K., Noge, H., Nakamura, Y., Inoshita, T., Shimizu, A. and Sakaki, H. (1994) *Phys. Rev. Lett*., Vol. 72, p.924.

97 Jiang, C., Muranaka, T. and Hasegawa, H. (2001) *Japan. J. Appl. Phys*., Vol. 40, p.3003.

98 Jiang, C. and Hasegawa, H. (2002) *Japan. J. Appl. Phys*., Vol. 41, p.972.

99 Chang, Y.C., Chang, L.L. and Esaki, L. (1985) *Appl. Phys. Lett*., Vol. 47, p.1324.

100 Akiyama, H. (1998) *J. Phys. Condens. Mat*., Vol. 10, p.3095.

101 Pfeiffer, L.N., West, K.W., Störmer, H.L., Eisenstein, J.P., Baldwin, K.W., Gershoni, D. and Spector, J. (1990) *Appl. Phys. Lett*., Vol. 56, p.1697.

102 Pfeiffer, L.N., Störmer, H.L., Baldwin, K.W., West, K.W., Goñi, A.R., Pinczuk, A., Ashoori, R.C., Dignam, M.M. and Wegscheider, W. (1993) *J. Cryst. Growth*, Vol. 127, p.849.

103 Gershoni, D., Weiner, J.S., Chu, G., S.N., Baraff, G.A., Vandenberg, J.M., Pfeiffer, L.N., West, K.W., Logan, R.A. and Tanbun-Ek, T. (1990) *Phys. Rev. Lett*., Vol. 65, p.1631.

104 Goñi, A.R., Pfeiffer, L.N., West, K.W., Pinczuk, A., Baranger, H.U. and Störmer, H.L. (1992) *Appl. Phys. Lett*., Vol. 61, p.1956.

105 Someya, T., Akiyama, H. and Sakaki, H. (1996) *J. Appl. Phys*., Vol. 79, p.2522.

106 Wegscheider, W., Pfeiffer, L.N., Dignam, M.M., Pinczuk, A., West, K.W., McCall, S.L. and Hull, R. (1993) *Phys. Rev. Lett*., Vol. 71, p.4071.

107 Wegscheider, W., Pfeiffer, L.N., West, K.W. and Leibenguth, R.E. (1994) *Appl. Phys. Lett*., Vol. 65, p.2510.

108 Wagner, R.S. and Ellis, W.C. (1964) *Appl. Phys. Lett*., Vol. 4, p.89.

109 Hiruma, K., Yazawa, M., Katsuyama, T., Ogawa, K., Haraguchi, K., Koguchi, M. and Kakibayashi, H. (1995) *J. Appl. Phys*., Vol. 77, p.447.

110 Yang, P., Wu, Y. and Fan, R. (2002) *Int. J. Nanosci*., Vol. 1, p.1.

111 Hu, J., Odom, T.W. and Lieber, C.M. (1999) *Acc. Chem. Res*., Vol. 32, p.435.

112 Wu, Y. and Yang, P. (2000) *Chem. Mater*., Vol. 12, p.605.

113 Morales, A.M. and Lieber, C.M. (1998) *Science*, Vol. 279, p.208.

114 Duan, X.F., Wang, J.F. and Lieber, C.M. (2000) *Appl. Phys. Lett*., Vol. 76, p.1116.

115 Trentler, T.J., Hickman, K.M., Geol, S.C., Viano, A.M., Gibbons, P.C. and Buhro, W.E. (1995) *Science*, Vol. 270, p.1791.

116 Martin, C.R. (1994) *Science*, Vol. 266, p.1961.

117 Braun, E., Eichen, Y., Sivan, U. and Ben-Yoseph, G. (1998) *Nature*, Vol. 391, p.775.

118 Vayssieres, L. (2004) *Int. J. Nanotech*., Vol. 1, Nos. 1/2, pp.1–41.

119 Mayers, B., Gates, B. and Xia, Y. (2004) *Int. J. Nanotech*., Vol. 1, Nos. 1/2, pp.86–104.

120 Maiman, T.H. (1960) *Nature*, Vol. 187, p.493.

121 Basov, N.G., Krokhin, O.N. and Popov, Y.M. (1961) *JETP*, Vol. 40, p.1320.

122 Hall, R.N., Fenner, G.E., Kingsley, J.D., Soltys, T.J. and Carlson, R.O. (1962) *Phys. Rev. Lett*., Vol. 9, p.366.

123 Nathan, M.I., Dumke, W.P., Burns, G., Dill, F.H. Jr. and Lasher, G.J. (1962) *Appl. Phys. Lett*., Vol. 1, p.62.

124 Holonyak Jr., N. and Bevacqua, S.F. (1962) *Appl. Phys. Lett*., Vol. 1, No. 82.

125 Quist, T.M., Rediker, R.H., Keyes, R.J., Krag, W.E., Lax, B., McWhorter, A.L. and Zeiger, H.J. (1962) *Appl. Phys. Lett*., Vol. 1, p.91.

126 Kroemer, H. (1963) *Proc. IEEE*, Vol. 51, p.1782.

127 Kroemer, H. (1963) *Semiconductor Laser with Electric Pumping*, U.S. Patent 3309553, August 16.

128 Alferov, Z.I. and Kazarinov, R.F. (1963) *Semiconductor Laser with Electric Pumping*, Inventor's Certificate 181737, March 30.

129 Alferov, Z.I., Andreev, V.M., Korolkov, V.I., Portnoi, E.L. and Tretyakov, N. (1969) *Sov. Phys. – Semicond*., Vol. 2, p.1289.

130 Alferov, Z.I., Andreev, V.M., Korolkov, V.I., Nikitin, V.G. and Yakovenko, A.A. (1971) *Sov. Phys. – Semicond*., Vol. 4, p.481.

131 Hayashi, I., Panish, M.B., Foy, W. and Sumski, S. (1970) *Appl. Phys. Lett*., Vol. 17, p.109.

132 Alferov, Z.I., Andreev, V.M., Korolkov, V.I., Tretyakov, D.N. and Tuchkevich, V.M. (1968) *Sov. Phys. – Semicond*., Vol. 1, p.1313.

133 Dingle, R., Wiegmann, W. and Henry, C.H. (1974) *Phys. Rev. Lett*., Vol. 33, p.827.

134 van der Ziel, J.P., Dingle, R., Miller, R.C., Wiegmann, W. and Nordland Jr., W.A. (1975) *Appl. Phys. Lett*., Vol. 26, p.463.

135 Dupuis, R.D., Dapkus, P.D., Holonyak, N. Jr., Rezek, E.A. and Chin, R. (1978) *Appl. Phys. Lett*., Vol. 32, p.295.

136 Chow, W.W., Choquette, K.D., Crawford, M.H., Lear, K.L. and Hadley, G.R. (1997) *IEEE J. Quantum Electron*., Vol. 33, p.1810.

137 Towe, E., Leheny, R.F. and Yang, A. (2000) *IEEE J. Sel. Top. Quantum Electron*., Vol. 6, p.1458.

138 Geels, R.S., Corzine, S.W., Scott, J.W., Young, D.B. and Coldren, L.A. (1990) *IEEE Photon. Tech. Lett*., Vol. 2, p.234.

139 Geels, R.S. and Coldren, L.A. (1990) *Appl. Phys. Lett*., Vol. 57, p.1605.

140 Levi, A.F.J., Slusher, R.E., McCall, S.L., Tanbun-Ek, T., Coblentz, D.L. and Pearton, S.J. (1992) *Electron. Lett*., Vol. 28, p.1010.

141 Levi, A.F.J., Slusher, R.E., McCall, S.L., Pearton, S.J. and Hobson, W.S. (1993) *Appl. Phys. Lett*., Vol. 62, p.2021.

142 Slusher, R.E., Levi, A.F.J., Mohideen, U., McCall, S.L., Pearton, S.J. and Logan, R.A. (1993) *Appl. Phys. Lett*., Vol. 63, p.1310.

143 Baba, T., Fujita, M., Sakai, A., Kihara, M. and Watanabe, R. (1997) *IEEE Photon. Tech. Lett*., Vol. 9, p.878.

144 Baba, T. (1997) *IEEE J. Sel. Top. Quantum Electron*., Vol. 3, p.808.

145 Faist, J., Capasso, F., Sivco, D.L., Sirtori, C., Hutchinson, A.L. and Cho, A.Y. (1994) *Science*, Vol. 264, p.553.

146 Scamarcio, G., Capasso, F., Sirtori, C., Faist, J., Hutchinson, A.L., Sivco, D.L. and Cho, A.Y. (1997) *Science*, Vol. 276, p.773.

147 Kazarinov, R. and Suris, R.A. (1971) *Sov. Phys. – Semicond*., Vol. 5, p.707.

148 Capasso, F., Gmachl, C., Paiella, R., Tredicucci, A., Hutchinson, A.L., Sivco, D.L., Baillargeon, J.N., Cho, A.Y. and Liu, H.C. (2000) *IEEE J. Sel. Top. Quantum Electron*., Vol. 6, p.931.

149 Capasso, F., Tredicucci, A., Gmachl, C., Sivco, D.L., Hutchinson, A.L., Cho, A.Y. and Scamarcio, G. (1999) *IEEE J. Sel. Top. Quantum Electron*., Vol. 5, p.792.

150 Cao, M., Miyake, Y., Tamura, S., Hirayama, H., Arai, S., Suematsu, Y. and Miyamoto, Y. (1990) *Trans. IEICE*, Vol. E73, p.63.

151 Cao, M., Daste, P., Miyamoto, M., Miyake, Y., Nogiwa, S., Arai, S., Furuya, K. and Suematsu, Y. (1988) *Electron. Lett*., Vol. 24, p.824.

152 Kojima, T., Tamura, M., Nakaya, H., Tanaka, S., Tamura, S. and Arai, S. (1998) *Japan. J. Appl. Phys*., Vol. 37, p.4792.

153 Yagi, H., Muranushi, K., Nunoya, N., Sano, T., Tamura, S. and Arai, S. (2002) *Japan. J. Appl. Phys*., Vol. 41, p.L186.

154 Nunoya, N., Yasumoto, H., Midorikawa, H., Tamura, S. and Arai, S. (2000) *Japan. J. Appl. Phys*., Vol. 39, p.L1042.

155 Nunoya, N., Nakamura, M., Morshed, M., Tamura, S. and Arai, S. (2001) *IEEE J. Sel. Top. Quantum Electron*., Vol. 7, p.249.

156 Nakamura, M., Nunoya, N., Yasumoto, H., Morshed, M., Fukuda, K., Tamura, S. and Arai, S. (2000) *Electron. Lett*., Vol. 36, p.639.

157 Yoshida, J. and Kishino, K. (1995) *IEEE Photon. Tech. Lett*., Vol. 7, p.241.

158 Chou, S.T., Wohlert, D.E., Cheng, K.Y. and Hsieh, K.C. (1998) *J. Appl. Phys*., Vol. 83, p.3469.

159 Wohlert, D.E. and Cheng, K.Y. and Chou, S.T. (2001) *Appl. Phys. Lett*., Vol. 78, p.1047.

160 Asada, M., Miyamoto, Y. and Suematsu, Y. (1985) *Japan. J. Appl. Phys*., Vol. 24, p.L95.

161 Tsuchiya, M., Petroff, P.M. and Coldren, L.A. (1989) *IEEE Trans. Electron. Dev*., Vol. 36, p.2612.

162 Hu, S.Y., Miller, M.S., Young, D.B., Yi, J.C., Leonard, D., Gossard, A.C., Petroff, P.M., Coldren, L.A. and Dagli, N. (1993) *Appl. Phys. Lett*., Vol. 63, p.2015.

163 Hu, S.Y., Yi, J.C., Miller, M.S., Leonard, D., Young, D.B., Gossard, A.C., Dagli, N., Petroff, P.M. and Coldren, L.A. (1995) *IEEE J. Quantum Electron*., Vol. 31, p.1380.

164 Saito, H., Uwai, K. and Kobayashi, N. (1993) *Japan. J. Appl. Phys*., Vol. 32, p.4440.

165 Hara, S., Motohisa, J. and Fukui, T. (1998) *Electron. Lett*., Vol. 34, p.894.

166 Ando, C.-P.H., Saito, H. and Kanbe, H. (1994) *Appl. Phys. Lett*., Vol. 64, p.1759.

167 Ohno, Y., Kanamori, H., Shimomura, S. and Hiyamizu, S. (2002) *Physica*, Vol. E13, p.892.

168 Kapon, E., Simhony, S., Bhat, R. and Hwang, D.M. (1989) *Appl. Phys. Lett*., Vol. 55, p.2715.

169 Tiwari, S., Pettit, G.D., Milkove, K.R., Legoues, F., Davis, R.J. and Woodall, J.M. (1994) *Appl. Phys. Lett*., Vol. 64, p.3536.

170 Qian, Y., Xu, Z.T., Zhang, J.M., Chen, L.H., Wang, Q.M., Zheng, L.X. and Hu, X.W. (1995) *Electron. Lett*., Vol. 3, p.102.

171 Piester, D., Bönsch, P., Schrimpf, T., Wehmann, H.-H. and Schlachetzki, A. (2000) *IEEE J. Sel. Top. Quantum Electron*., Vol. 6, p.522.

172 Kim, T.G., Son, C.S. and Ogura, M. (2001) *IEEE Photon. Tech. Lett*., Vol. 13, p.409.

173 Sirigu, L., Oberli, D.Y., Degiorgi, L., Rudra, A. and Kapon, E. (2000) *Phys. Rev*., Vol. B61, p.R10575.

174 Kim, T.G., Wang, X.-L., Kaji, R. and Ogura, M. (2000) *Physica*, Vol. E7, p.508.

175 Watanabe, S., Koshiba, S., Yoshita, M., Sakaki, H., Baba, M. and Akiyama, H. (1998) *Appl. Phys. Lett*., Vol. 73, p.511.

176 Watanabe, S., Koshiba, S., Yoshita, M., Sakaki, H., Baba, M. and Akiyama, H. (1999) *Appl. Phys. Lett*., Vol. 75, p.2190.

177 Sorba, L., Schedelbeck, G., Wegscheider, W., Bichler, M. and Abstreiter, G. (2000) *Phys. Stat. Sol*., Vol. A178, p.227.

178 Hayamizu, Y., Yoshita, M., Watanabe, S., Akiyama, H., Pfeiffer, L.N. and West, K.W. (2002) *Appl. Phys. Lett*., Vol. 81, p.4937.

179 Fons, P., Iwata, K., Yamada, A., Matsubara, K., Niki, S., Nakahara, K., Tanabe, T. and H.Takasu (2000) *Appl. Phys. Lett*., Vol. 77, p.1801.

180 Bagnall, D.M., Chen, Y.F., Zhu, Z., Yao, T., Koyama, S., Shen, M.Y. and Goto, T. (1997) *Appl. Phys. Lett*., Vol. 70, p.2230.

181 Yu, P., Tang, Z.K., Wong, L., G.K., Kawasaki, M., Ohtomo, A., Koinuma, H. and Segawa, Y. (1998) *J. Cryst. Growth*, Vol. 184, p.601.

182 Cao, H. *et al.* (2000) *Phys. Rev. Lett*., Vol. 84, p.5584.

183 Yang, P., Yan, H., Mao, S.S., Russo, R.E., Johnson, J.C., Saykally, R.J., Morris, N., Pham, J., He, R. and Choi, H.J. (2002) *Adv. Func. Mater*., Vol. 12, p.323.

184 Johnson, J.C., Yan, H., Schaller, R.D., Haber, L.H., Saykally, R.J. and Yang, P. (2001) *J. Phys. Chem.*, Vol. B105, p.11387.

185 Johnson, J.C., Choi, H.J., Knutsen, K.P., Schaller, R.D., Yang, P. and Saykally, R.J. (2002) *Nature Mater*., Vol. 1, p.106.

186 Duan, X., Huang, Y., Agarwal, R. and Lieber, C.M. (2003) *Nature*, Vol. 421, p.241.

187 Kirstaedter, N., Ledentsov, N.N., Grundmann, M., Bimberg, D., Ustinov, V.M., Ruvimov, S.S., Maximov, M.V., Kopev, P.S. and Alferov, Z.I. (1994) *Electron. Lett*., Vol. 30, p.1416.

188 Hirayama, H., Matsunaga, K., Asada, M. and Suematsu, Y. (1994) *Electron. Lett*., Vol. 30, p.142.

189 Michler, P., Imamoglu, A., Mason, M.D., Carson, P.J., Strouse, G.F. and Buratto, S.K. (2000) *Nature*, Vol. 406, p.968.

190 Michler, P., Kiraz, A., Becher, C., Schoenfeld, W.V., Petroff, P.M., Zhang, L., Hu, E. and Imamoglu, A. (2000) *Science*, Vol. 290, p.2282.

191 Santori, C., Pelton, M., Solomon, G., Dale, Y. and Yamamoto, Y. (2001) *Phys. Rev. Lett*., Vol. 86, p.1502.

192 Bauer, E. and Poppa, H. (1972) *Thin Solid Films*, Vol. 12, p.167.

193 Eaglesham, D.J. and Cerullo, M. (1990) *Phys. Rev. Lett*., Vol. 64, p.1943.

194 Leonard, D., Krishnamurthy, M., Reaves, C.M., Denbaars, S.P. and Petroff, P.M. (1993) *Appl. Phys. Lett*., Vol. 63, p.3203.

195 Moison, J.M., Houzay, F., Barthe, F., Leprince, L., Andre, E. and Vatel, O. (1994) *Appl. Phys. Lett*., Vol. 64, p.196.

196 Shchukin, V.A., Ledenstov, N.N., Kopev, P.S. and Bimberg, D. (1995) *Phys. Rev. Lett*., Vol. 75, p.2968.

197 Rossetti, R., Nakahara, S. and Brus, L.E. (1983) *J. Chem. Phys*., Vol. 79, p.1986.

198 Alivisatos, A.P., Harris, A.L., I.evinos, N.J., Steigerwald, M.L. and Brus, L.E. (1988) *J. Chem. Phys*., Vol. 89, p.4001.

199 Steigerwald, M.L. and Brus, L.E. (1989) *Ann. Rev. Mater. Sci*., Vol. 19, p.471.

200 Bawendi, M.G., Carroll, P.J., Wilson, L. and Brus, L.E. (1992) *J. Chem. Phys*., Vol. 96, p.946.

201 Murray, C.B., Norris, D.J. and Bawendi, M.G. (1993) *J. Am. Chem. Soc*., Vol. 115, p.8706.

202 Katari, J.E.B., Colvin, V.L. and Alivisatos, A.P. (1994) *J. Phys. Chem*., Vol. 98, p.4109.

203 Murray, C.B., Kagan, C.R. and Bawendi, M.G. (2000) *Annu. Rev. Mater. Sci*., Vol. 30, p.545.

204 Alivisatos, A.P. (1996) *Science*, Vol. 271, p.933.

205 Bimberg, D., Grundmann, M. and Ledentsov, N.N. (1999) *Quantum Dot Heterostructures*, Wiley, New York.

206 Rennon, S., Avary, K., Klopf, F., Reithmaier, J.P. and Forchel, A. (2001) *IEEE J. Sel. Top. Quantum Electon*., Vol. 7, p.300.

207 Saito, H., Nishi, K., Ogura, I., Sugou, S. and Sugimoto, Y. (1996) *Appl. Phys. Lett*., Vol. 69, p.3140.

208 Lott, J.A., Ledentsov, N.N., Ustinov, V.M., Egorov, A.Y., Zhukov, A.E., Kopev, P.S., Alferov, Z.I. and Bimberg, D. (1997) *Electron. Lett*., Vol. 33, p.1150.

209 Yoshie, T., Shchekin, O.B., Chen, H., Deppe, D.G. and Scherer, A. (2002) *Electron. Lett*., Vol. 38, p.967.

210 Michler, P., Kiraz, A., Zhang, L., Becher, C., Hu, E. and Imamoglu, A. (2000) *Appl. Phys. Lett*., Vol. 77, p.184.

211 Young, D.K., Zhang, L., Awschalom, D.D. and Hu, E.L. (2002) *Phys. Rev*., Vol. B66, p.R81307.

212 Sellin, R., Ribbat, C., Grundmann, M., Ledentsov, N.N. and Bimberg, D. (2001) *Appl. Phys. Lett*., Vol. 78, p.1207.

213 Kim, H.J., Motohisa, J. and Fukui, T. (2002) *Appl. Phys. Lett*., Vol. 81, p.5147.

214 Ogawa, T. and Takagahara, T. (1991) *Phys. Rev*., Vol. B44, p.8138.

215 Nojima, S. (1994) *Phys. Rev*., Vol. B50, p.2306.

216 Grundmann, M. and Bimberg, D. (1997) *Phys. Rev*., Vol. B55, p.4054.

217 Rossi, F., Goldoni, G. and Molinari, E. (1997) *Phys. Rev. Lett*., Vol. 78, p.3527.

218 Sarma, S.D. and Wang, D.W. (2000) *Phys. Rev. Lett*., Vol. 84, p.2010.

219 Kuther, A., Bayer, M., Gutbrod, T., Forchel, A., Knipp, P.A. Reinecke, T.L. and Werner, R. (1998) *Phys. Rev*., Vol. B58, p.15744.

220 Constantin, C., Martinet, E., Oberli, D.Y., Kapon, E., Gayral, B. and Gerard, J.-M. (2002) *Phys. Rev*., Vol. B66, p.165306.

221 Vuckovic, J., Pelton, M., Scherer, A. and Yamamoto, Y. (2002) *Phys. Rev*., Vol. A66, p.23808.

222 Yamamoto, Y., Tassone, F. and Cao, H. (2000) *Semiconductor Cavity Quantum Electrodynamics*, Springer, Berlin, 2000.